Kobielak, A., and Fuchs, E. (2004). Alpha-catenin: at the junction of intercellular adhesion and actin dynamics. Nat. Rev. Mol. Cell Biol. *5*, 614–625.

Kooistra, M. R., Corada, M., Dejana, E., and Bos, J. L. (2005). Epac1 regulates integrity of endothelial cell junctions through VE-cadherin. FEBS Lett. *579*, 4966–4972.

Kotelevets, L., van Hengel, J., Bruyneel, E., Mareel, M., van Roy, F., and Chastre, E. (2005). Implication of the MAGI-1b/PTEN signalosome in stabilization of adherens junctions and suppression of invasiveness. FASEB J. *19*, 115–117.

Laura, R. P., Ross, S., Koeppen, H., and Lasky, L. A. (2002). MAGI-1, a widely expressed, alternatively spliced tight junction protein. Exp. Cell Res. *275*, 155–170.

Mandell, K. J., Babbin, B. A., Nusrat, A., and Parkos, C. A. (2005). Junctional adhesion molecule 1 regulates epithelial cell morphology through effects on beta1 integrins and Rap1 activity. J. Biol. Chem. *280*, 11665–11674.

Mino, A., Ohtsuka, T., Inoue, E., and Takai, Y. (2000). Membrane-associated guanylate kinase with inverted orientation (MAGI)-1/brain angiogenesis inhibitor 1-associated protein (BAP1) as a scaffolding molecule for Rap small G protein GDP/GTP exchange protein at tight junctions. Genes Cells *5*, 1009–1016.

Mochizuki, N., Yamashita, S., Kurokawa, K., Ohba, Y., Nagai, T., Miyawaki, A., and Matsuda, M. (2001). Spatio-temporal images of growth-factor-induced activation of Ras and Rap1. Nature *411*, 1065–1068.

Nagashima, K., Endo, A., Ogita, H., Kawana, A., Yamagishi, A., Kitabatake, A., Matsuda, M., Mochizuki, N. (2002). Adaptor protein Crk is required for Ephrin-B1-induced membrane ruffling and focal complex assembly of human aortic endothelial cells. Mol. Biol. Cell *13*, 4231–4242.

Navarro, P., Ruco, L., and Dejana, E. (1998). Differential localization of VE- and N-cadherins in human endothelial cells: VE-cadherin competes with N-cadherin for junctional localization. J. Cell Biol. *140*, 1475–1484.

Nwariaku, F. E., Liu, Z., Zhu, X., Nahari, D., Ingle, C., Wu, R. F., Gu, Y., Sarosi, G., and Terada, L. S. (2004). NADPH oxidase mediates vascular endothelial cadherin phosphorylation and endothelial dysfunction. Blood *104*, 3214–3220.

Ohba, Y. *et al.* (2001). Requirement for C3G-dependent Rap1 activation for cell adhesion and embryogenesis. EMBO J. *20*, 3333–3341.

Price, L. S., Hajdo-Milasinovic, A., Zhao, J., Zwartkruis, F. J., Collard, J. G., and Bos, J. L. (2004). Rap1 regulates E-cadherin-mediated cell-cell adhesion. J. Biol. Chem. *279*, 35127–35132.

Subauste, M. C., Nalbant, P., Adamson, E. D., and Hahn, K. M. (2005). Vinculin controls PTEN protein level by maintaining the interaction of the adherens junction protein beta-catenin with the scaffolding protein MAGI-2. J. Biol. Chem. *280*, 5676–5681.

Tachibana, K., Nakanishi, H., Mandai, K., Ozaki, K., Ikeda, W., Yamamoto, Y., Nagafuchi, A., Tsukita, S., and Takai, Y. (2000). Two cell adhesion molecules, nectin and cadherin, interact through their cytoplasmic domain-associated proteins. J. Cell Biol. *150*, 1161–1176.

Tanaka, Y., Nakanishi, H., Kakunaga, S., Okabe, N., Kawakatsu, T., Shimizu, K., and Takai, Y. (2003). Role of nectin in formation of E-cadherin-based adherens junctions in keratinocytes: analysis with the N-cadherin dominant negative mutant. Mol. Biol. Cell *14*, 1597–1609.

Volberg, T., Geiger, B., Kartenbeck, J., and Franke, W. W. (1986). Changes in membrane-microfilament interaction in intercellular adherens junctions upon removal of extracellular Ca2+ ions. J. Cell Biol. *102*, 1832–1842.

Wittchen, E. S., Worthylake, R. A., Kelly, P., Casey, P. J., Quilliam, L. A., and Burridge, K. (2005). Rap1 GTPase inhibits leukocyte transmigration by promoting endothelial barrier function. J. Biol. Chem. *280*, 11675–11682.

Yamada, A., Irie, K., Hirota, T., Ooshio, T., Fukuhara, A., and Takai, Y. (2005). Involvement of the annexin II-S100A10 complex in the formation of E-cadherin-based adherens junctions in Madin-Darby canine kidney cells. J. Biol. Chem. *280*, 6016–6027.

Zanetti, A., Lampugnani, M. G., Balconi, G., Breviario, F., Corada, M., Lanfrancone, L., and Dejana, E. (2002). Vascular endothelial growth factor induces SHC association with vascular endothelial cadherin: a potential feedback mechanism to control vascular endothelial growth factor receptor-2 signaling. Arterioscler. Thromb. Vasc. Biol. 22, 617–622.

Available online at www.sciencedirect.com
SCIENCE DIRECT®
ELSEVIER
Cellular Signalling xx (2005) xxx–xxx
CELLULAR SIGNALLING
www.elsevier.com/locate/cellsig

ERK is an anti-inflammatory signal that suppresses expression of NF-κB-dependent inflammatory genes by inhibiting IKK activity in endothelial cells

Yong-Sun Maeng [a,1], Jeong-Ki Min [a,1], Jeong-Hun Kim [b], Akiko Yamagishi [c], Naoki Mochizuki [c], Ja-Young Kwon [d], Yong-Won Park [d], Young-Myeong Kim [e], Young-Guen Kwon [a,*]

[a] *Department of Biochemistry College of Sciences, Yonsei University, Seoul 120-749, Korea*
[b] *Department of Ophthalmology Seoul National University College of Medicine, Seoul Artificial Eye Center, Clinical Research Institute, Seoul National University Hospital, Seoul 110-744, Korea*
[c] *Department of Structural Analysis, National Cardiovascular Center Research Institute, 5-7-1 Fujishirodai, Suita, Osaka 565-8565, Japan*
[d] *Department of Obstetrics and Gynecology Yonsei University College of Medicine 134 Shinchon-dong, Seodaemoon-gu Seoul 120-752, Korea*
[e] *Department of Molecular and Cellular Biochemistry, School of Medicine, Kangwon National University, Chunchon, Kangwon-Do 200-701, Korea*

Received 29 July 2005; received in revised form 20 August 2005; accepted 22 August 2005

Abstract

Unveiling of endothelial nuclear factor-κB (NF-κB) activation is pivotal for understanding the inflammatory reaction and the pathogenesis of inflammatory vascular diseases. We here report the novel function of extracellular signal-related kinase (ERK) in controlling endothelial NF-κB activation and inflammatory responses. In human endothelial cells, vascular endothelial growth factor (VEGF) induced NF-κB-dependent transcription of cell adhesion molecules (CAMs) and monocyte adhesion. These effects were prominently enhanced by either pretreatment with the MEK inhibitors, PD98059 and U0126 or overexpression of a dominant negative form of MEK, but blocked by a wild type ERK. Consistently, inhibition of ERK significantly increased IκB kinase (IKK) activity, IκBα phosphorylation, and nuclear translocation of NF-κB induced by VEGF, whereas overexpression of ERK resulted in the loss of these responses to VEGF. Using two PKC inhibitors has demonstrated that VEGF concomitantly stimulates IKK and its negative regulatory signal ERK through PKC that lies downstream of KDR/Flk. Strikingly, elevation of ERK in endothelial cells markedly inhibited CAM expression and NF-κB activation as well as monocyte adhesion induced by IL-1β and TNF-α. The data collectively suggest that ERK serves as an anti-inflammatory signal that suppresses expression of NF-κB-dependent inflammatory genes by inhibiting IKK activity in endothelial cells. Measuring the existence of ERK activity in vascular endothelial cells may be useful for predicting the feasibility and potency of inflammatory reactions in the vasculature.

Keywords: VEGF; ERK; NF-κB; CAMs; Inflammation

1. Introduction

Inflammatory conditions are characterized by the migration of proliferating leucocytes from the blood to the tissues and involve a coordinated series of adhesion processes between circulating and resident leukocytes and the vascular endothelium [1–3]. These events are controlled by different types of adhesion molecules on the leukocytes and endothelium [3]. In particular, expression of cell adhesion molecules (CAMs), such as E-selectin, intercellular adhesion molecule-1 (ICAM-1), and vascular cell adhesion molecule-1 (VCAM-1),

Abbreviations: VEGF, vascular endothelial growth factor; HUVECs, human umbilical vein endothelial cells; bFGF, basic fibroblast growth factor; EGF, epidermal growth factor; TNF-α, tumor necrosis factor-α; IL-1β, interleukin-1β; KDR, Flk-1/kinase-insert domain containing receptor; VCAM-1, vascular cell adhesion molecule-1; ICAM-1, intercellular adhesion molecule-1; PI3K, phosphatidylinositol 3′-kinase; PLC, phospholipase C; PKC, protein kinase C; IKK, IκB kinase; MEK, mitogen-activated protein/extracellular signal-regulated kinase kinase; ERK, extracellular signal-regulated kinase; RT-PCR, reverse transcriptase-polymerase chain reaction.

* Corresponding author. Tel.: +82 2 2123 5697; fax: +82 2 362 9897.
E-mail address: ygkwon@yonsei.ac.kr (Y.-G. Kwon).
[1] These authors contributed equally to this study.

0898-6568/$ - see front matter © 2005 Elsevier B.V. All rights reserved.
doi:10.1016/j.cellsig.2005.08.007

on the surface of endothelial cells is required for endothelial–leukocyte cell interaction [1]. In the absence of inflammation, CAM expression is low on the endothelial cells of most vascular beds, but it dramatically increases in response to a number of extracellular stimuli, including tumor necrosis factor-α (TNF-α), interleukin-1β (IL-1β), vascular endothelial growth factor (VEGF), and bacterial lipopolysaccharides [4–6]. Among the classical transcription factors activated by inflammatory cytokines, nuclear factor-κB (NF-κB) plays a pivotal role in the regulation of inflammatory response genes [7,8]. Indeed, it is considered to be a major transcriptional regulator of CAMs in endothelial cells [9].

In mammalian, the five members of the NF-κB family, p65 (RelA), RelB, c-Rel, p50/p105 (NF-κB1), and p52/p100 (NF-κB2), exist in quiescent cells as homo- or heterodimers bound to IκB family proteins and retained in the cytoplasm as an inactive state [10]. In stimulated cells, IκB is degraded through the ubiquitin-proteasome pathway upon specific phosphorylation by activated IκB kinase (IKK) [11]. The IKK activity in cells can be purified as a 700–900-kDa complex, and has been shown to contain two kinase subunits, IKKα (IKK1) and IKKβ (IKK2), and a regulatory subunit, NEMO (NF-κB essential modifier) or IKKγ [11–13]. In the canonical NF-κB signaling pathway, IKKβ is both necessary and sufficient for phosphorylation of IκBα on Ser 32 and Ser 36, and IκBβ on Ser 19 and Ser 23 [12]. By contrast, although the role of IKKα in the canonical pathway is unclear, recent studies suggest that the IKKα subunit phosphorylates p100 and causes its inducible processing to p52 [13].

The activation of the IKK complex is suggested to be exerted by phosphorylation of the IKK complex by the mitogen-activated protein kinase kinase kinase (MAP3K) family including NF-κB-inducing kinase [14], mitogen-activated protein/ERK kinase kinase 1 (MEKK) [15], MEKK3 [16], TGF-β activating kinase 1 [17] and NF-κB-activating kinase [18]. The MAP3K family phosphorylated and induced NF-κB activation when overexpressed or when assayed in vitro, but the mechanism by which cytokines lead to the activation of the IKK complex in vivo is still controversial [19]. Alternatively, previous studies have also suggested that IKK recruitment to receptor complexes at the cell membrane results in its autophosphorylation and subsequent activation [20]. Indeed, IKK recruitment to the TNF receptor-1 complex is shown to be required for TNFα-mediated activation of the IKK complex [11,21–23]. In addition, the important involvement of various intracellular adaptors such as TNF-receptor-associated factors and death-domain kinase receptor-interacting protein in receptor-mediated NF-κB pathway has been extensively reported [24]. However, despite of a large number of studies in vitro and in vivo, the specific upstream signaling mechanism that regulates the IKK activity remains for further investigation.

In the present study, we report an important regulatory role of extracellular signal-related kinase (ERK) in controlling expression of NF-κB-dependent inflammatory genes in vascular endothelial cells. We found that inhibition of ERK markedly increased CAM expression in response to VEGF, which induces both ERK and NF-κB activation in endothelial cells, and this effect was correlated with increased NF-κB activation. Furthermore, elevation of ERK activity in endothelial cells resulted in the suppression of CAM expression and NF-κB activation as well as leukocyte adhesion induced by IL-1β and TNF-α in addition to VEGF. We therefore propose that ERK is a potential intracellular regulator that suppresses vascular inflammation by inhibiting NF-κB activation in endothelial cells.

2. Materials and methods

2.1. Cell culture and reagents

Human umbilical vein endothelial cells (HUVECs) were isolated from human umbilical cord veins by collagenase treatment as described previously [25] and used in passages 2–7. The cells were grown in M199 medium (Invitrogen, Carlsbad, CA) supplemented with 20% fetal bovine serum, 100 units/ml penicillin, 100 G μ/ml streptomycin, 3 ng/ml bFGF (Upstate Biotechnology, Lake Placid, NY), and 5 units/ml heparin at 37 °C in humidified 5% CO2/95% air. U937 cells were grown in RPMI-1640 (Invitrogen). VEGF was from Upstate Biotechnology (Lake Placid, NY), PD98059 from Alexis (San Diego, CA), and U0126 and GF109203X from BIOMOL (Plymouth Meeting, PA). Chelerythrine chloride and actinomycin D were from Sigma. M199, heparin, Trizol reagent and LipofectAMINE Plus were purchased from Invitrogen. Antibodies used were as follows: rabbit anti-VCAM-1 polyclonal antibody, mouse anti-actin monoclonal antibody (Santa Cruz Biotechnology, SantaCruz, Calif), rabbit anti-phospho-IκB-α polyclonal antibody (Cell Signaling, Beverly, MA), mouse anti-phospho-ERK (Thr-202/Tyr-204) monoclonal antibody, and rabbit anti-ERK polyclonal antibody (New England Biolabs, Beverly, MA). All other reagents were purchased from Sigma unless otherwise indicated.

2.2. Construction of reporter plasmids

The VCAM-1 luciferase plasmids were constructed as described previously [26]. The human VCAM-1 promoter, spanning 1716 to +119 bp, was amplified by PCR with primers containing 5′ *KpnI* and 3′ *Xho*I restriction sites. The resulting PCR fragment was digested with *Kpn*I and *Xho*I and cloned into pGL3-basic vector (Promega). Synthetic oligonucleotide sense and antisense primers were used to generate a series of DNA fragments with successive 5′ deletions. All PCR products were digested with *KpnI* and *XhoI* and cloned into pGL3-basic vector. The following deletion constructs of the human VCAM-1 promoter were generated: 1716 to +119 bp (fragment 6), 366 to +119 bp (fragment 5), 296 to +119 bp (fragment 4), 210 to +119 bp fragment 3) and 38 to +119 bp (fragment 2). To construct the ICAM-1 luciferase plasmid, we cloned regions spanning −1350 to +45 bp of the human ICAM-1 promoter into pGL3-basic vector (Promega). Plasmid DNAs were purified from bacterial cultures using an Endofree Plasmid Maxi kit (Qiagen, Chatsworth, CA). We confirmed all constructs by restriction enzyme mapping and sequencing.

2.3. Transfections and analysis of luciferase activity

HUVECs were transfected with 1 μg of the above plasmids and 1 μg of the control pCMV-β-gal plasmid using LipofectAMINE Plus reagents (Invitrogen, Carlsbad, CA). Cell extracts were prepared twenty-four hours after transfection, and luciferase assays carried out with the Luciferase Assay System (Promega). Luciferase activities were normalized with respect to parallel β-galactosidase activities, to correct for differences in transfection efficiency, and the β-galactosidase assays were performed using the β-Galactosidase Enzyme Assay System (Promega). Each experimental point was performed in at least quadruplicate.

2.4. Flow cytometry

Cells from subconfluent cultures were detached gently from plates with PBS containing 2 mM EDTA. The cells were washed two or three times with PBS, resuspended in PBS containing 3% bovine serum albumin and incubated with FITC-conjugated VCAM-1 antibody (Serotec) for 30 min on ice. They were then fixed with 2% paraformaldehyde and analyzed by flow cytometry in a fluorescence-activated cell sorter (Becton Dickinson). Each experimental condition was performed in quadruplicate.

2.5. Semi-quantitative RT-PCR analysis

Total RNA was obtained from HUVECs with a TRIzol reagent kit. 0.5–5 μg RNA samples were used in the reverse transcriptase-polymerase chain reactions (RT-PCR), and the correlation between the amounts of RNA used and quantity of PCR products from VCAM-1 mRNA and the internal standard (β-actin) mRNA was examined. Briefly, target RNA was converted to cDNA by treatment with 200 units of reverse transcriptase and 500 ng of oligo(dT) primer in 50 mM Tris–HCl (pH 8.3), 75 mM KCl, 3 mM $MgCl_2$, 10 mM dithiothreitol, and 1 mM dNTPs at 42 °C for 1 h. The reaction was stopped by heating at 70 °C for 15 min. One μl of the cDNA mixture was used for enzymatic amplification. The polymerase chain reaction was performed in 50 mM KCl, 10 mM Tris–HCl (pH 8.3), 1.5 mM $MgCl_2$, 0.2 mM dNTPs, 2.5 units of *Taq* DNA polymerase, and 0.1 μM of primers for VCAM-1. Amplification was performed in a DNA thermal cycler (model PTC-200; MJ Research) under the following condition: denaturation at 94 °C for 5 min for the first cycle and for 30 s thereafter, annealing at 60 °C (VCAM-1), for 30 s, and extension at 72 °C for 30 s for 25 repetitive cycles. Final extension was at 72 °C for 10 min. The primers used for VCAM-1 were as follows: 5′-GATACAACCGTCTTGGTCAGCCC-3′ (sense) and 5′CGC-ATCCTTCAACTGGCCTT-3′ (antisense). Each experimental condition was performed in quadruplicate.

2.6. Transfer vector constructs

HIV-vectors were produced from the previously described SIN-18 vector, which contains a large deletion in the U3 region of the 3′ long terminal repeat (LTR) [27]. The SIN.cPPT.CMV-EGFP-W vector contained the enhanced green fluorescent protein (EGFP) transgene driven by the human cytomegalovirus (CMV) immediate-early enhancer/promoter. The SIN.cPPT.ERK2-EGFP-W vector contained the human extracellular signal-related kinase 2 gene.

2.7. Lentiviral vectors and in vitro gene transfer

VSV-G-pseudotyped, HIV-1-based vector particles were produced by cotransfection of four plasmids (pMDLg/pRRE: 12 μg; pRSVrev: 3 μg; pMD.G: 5 μg, SIN vector: 20 μg) onto 293T cells. Culture medium was replaced by serum-free SFM-II medium (Invitrogen) 15 h post-transfection. Thirty-two hours later, cell supernatants were harvested, filtered through a 0.45 μm filtration system, concentrated on Centricon Plus-80 Biomax MW 100,000 (Millipore, Le-Mont-sur-Lausanne, Switzerland), resuspended in PBS, and re-concentrated on Centricon-20. The titer of the SIN.cPPT.CMV-EGFP-W vector stock solution was 5×10^9 transducing units (TU)/ml by flow cytometry on 293T cells, and 3×10^4 ng p24 antigen per ml by p24-ELISA. The SIN.cPPT.ERK2-EGFP-W vector was titered by flow cytometry on HUVECs (of note, titration of SIN.cPPT.CMV-EGFP-W yielded similar results in HUVECs and 293T cells). HUVECs were seeded in six-well plates and allowed to adhere overnight. Viral vectors were added to cell cultures at varying multiplicities of infection (MOIs ≈1–50). At 18 h, cells were washed and medium was replaced. Cells were harvested at the indicated time points. Percentages of EGFP-positive cells and their mean fluorescence values (MFVs) were determined by flow cytometry (FACScan).

2.8. Preparation of nuclear extracts and electrophoretic mobility shift assays

Cells were washed three times with ice-cold Tris-buffered saline (TBS) and resuspended in 400 μl of buffer A [10 mM HEPES (pH 7.9), 10 mM KCl, 0.1 mM EDTA, 0.1 mM EGTA, 1 mM dithiothreitol (DTT), 1 mM phenylmethylsulfonyl fluoride (PMSF), 5 μg/mL of leupeptin, and 5 μg/mL of aprotinin]. After 15 min, Nonidet P-40 (NP-40) was added to a final concentration of 0.6%. Nuclei were pelleted and suspended in 50 μl of buffer C [20 mM HEPES (pH 7.9), 0.4 M NaCl, 1 mM EDTA, 1 mM EGTA, 1 mM DTT, 1 mM PMSF, 5 μg/ml of leupeptin, and 5 μg/ml of aprotonin]. After 30 min agitation at 4 °C, the lysates were centrifuged, and the supernatants containing the nuclear proteins were diluted with buffer C. Binding reactions contained 15 μg of nuclear protein and a ^{32}P end-labeled, double-stranded oligonucleotide containing the NF-κB binding site on the human VCAM-1 promoter (5′-CCTTGAAGGGATTTCCCTCC-3′) and were incubated for 30 min. Cold competition controls were performed by preincubating the nuclear proteins with a 20-fold molar excess of unlabeled NF-κB double-stranded oligonucleotide for 20 min. The mixtures were resolved on native 5% polyacrylamide gels, which were dried and autoradiographed.

Each experimental point was performed in duplicate and represents several independent conditions.

2.9. In vitro kinase assays

IKK was assayed as described previously [28]. Briefly, the IKK complex was precipitated from whole cell extracts with antibody against IKK-γ, followed by treatment with protein A-Sepharose beads (Pierce). After a 2 h incubation, the beads were washed with lysis buffer and assayed in kinase assay mixture containing 50 mM HEPES (pH 7.4), 20 mM $MgCl_2$, 2 mM dithiothreitol, 20 Ci μof [γ-^{32}P]ATP, 10 μM unlabeled ATP, and 2 μg of substrate GST-IκBα (amino acids 1–54). After incubation at 30 °C for 30 min, the reaction was terminated by boiling in SDS sample buffer for 5 min. Finally, the protein was resolved on 10% SDS-PAGE, the gel was dried, and the radioactive bands were visualized with a PhosphorImager. To determine the total amounts of IKK complex in each sample, 50 μg of whole cell protein was resolved on 7.5% SDS-PAGE, electrotransferred to a nitrocellulose membrane, and blotted with anti-IKK-γ antibody. The data represent the average of two separate experiments, each performed in duplicate.

2.10. Immunocytochemical localization of p65

Nuclear translocation of the p65 subunit of NF-κB was examined by an immunocytochemical method as described previously [28]. Briefly, treated cells were fixed with 2% paraformaldehyde and permeabilized with 0.2% Triton X-100. After washing in phosphate-buffered saline, the slides were blocked with 3% bovine serum albumin for 1 h and the cells incubated with goat polyclonal anti-p65 antibody (Santa Cruz

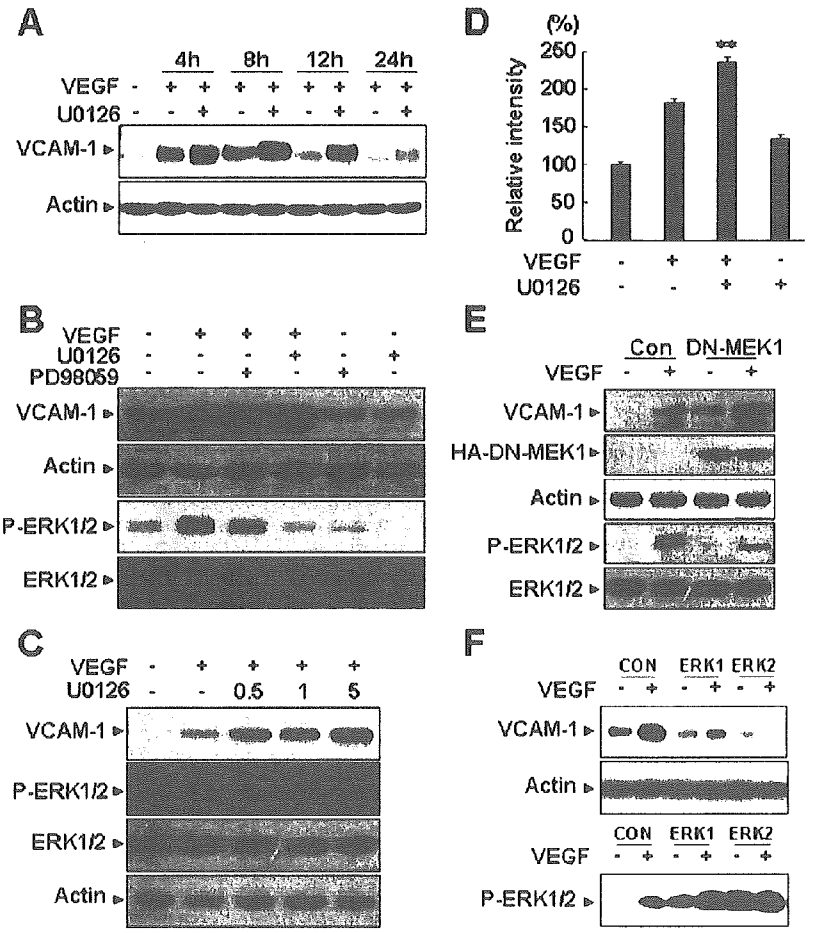

Fig. 1. Inhibition of ERK resulted in increased expression of VCAM-1 in response to VEGF. (A) HUVECs were incubated for 30 min with or without 5 μM U0126 and stimulated with 10 ng/ml VEGF for the indicated times. (B) HUVECs were pretreated for 30 min with 5 μM U0126 or 10 μM PD98059 prior to stimulation with 10 ng/ml VEGF for 10 min (*lower panel*) or 8 h (*upper panel*). (C) HUVECs were incubated for 30 min with or without various concentrations of U0126 and stimulated with 10 ng/ml VEGF for 10 min (*lower panel*) or 8 h (*upper panel*). Western blots were probed with anti-VCAM-1 antibody and an anti-phospho-ERK antibody, and reprobed with anti-actin antibody or anti-ERK antibody to verify equal loading of proteins. (D) HUVECs were pretreated for 30 min with 5 μM U0126 and then stimulated with 10 ng/ml VEGF for 8 h. The cells were detached from the plates, treated with FITC-conjugated VCAM-1 antibody and analyzed with a FACScan. Staining was quantified by flow cytometry. HUVECs were transfected with hemagglutinin (HA) tagged dominant negative form of MEK1, DN-MEK1, (E) or a wild form of ERKs (ERK1, 2) (F) and then stimulated with VEGF (10 ng/ml) for 10 min (*lower panel*) or 8 h (*upper panel*). Western blots were probed with anti-VCAM-1, anti-HA, and anti-phospho-ERK antibody and reprobed with anti-actin antibody or anti-ERK antibody to verify equal loading of proteins. Con indicates cells transfected with empty vector. **, $P<0.01$ versus VEGF alone.

Biotechnology, Santa Cruz, CA) (1 : 100). After 2 h at 4 °C the cells were washed and incubated with anti-goat IgG-rhodamine (Santa Cruz) (1 : 100) for 1 h. The cells were then mounted with mounting medium and observed with a fluorescence microscope (Olympus).

2.11. Adhesion assays

HUVECs were plated on 2% gelatin-coated 96-well plates at a density of 1×10^4 cells/well and stimulated with VEGF for 8 h. Human U937 cells were then added (5×10^4 cells/ml, 200 μl/well) to the confluent HUVEC monolayers and incubated for 30 min. Thereafter the cells in the wells were washed out 3 times with PBS, fixed and stained with Diff-Quick (Baxter Healthcare Corp., McGraw Park, IL). The adherent cells in 5 randomly selected optical fields of each well were counted. Each experimental point was performed in duplicate and represents several independent conditions.

2.12. Western blotting

Cell lysates or immunoprecipitates were fractionated by SDS-PAGE and transferred to polyvinyldifluoride membranes. The blocked membranes were incubated with the appropriate antibody, and the immunoreactive bands were visualized with a

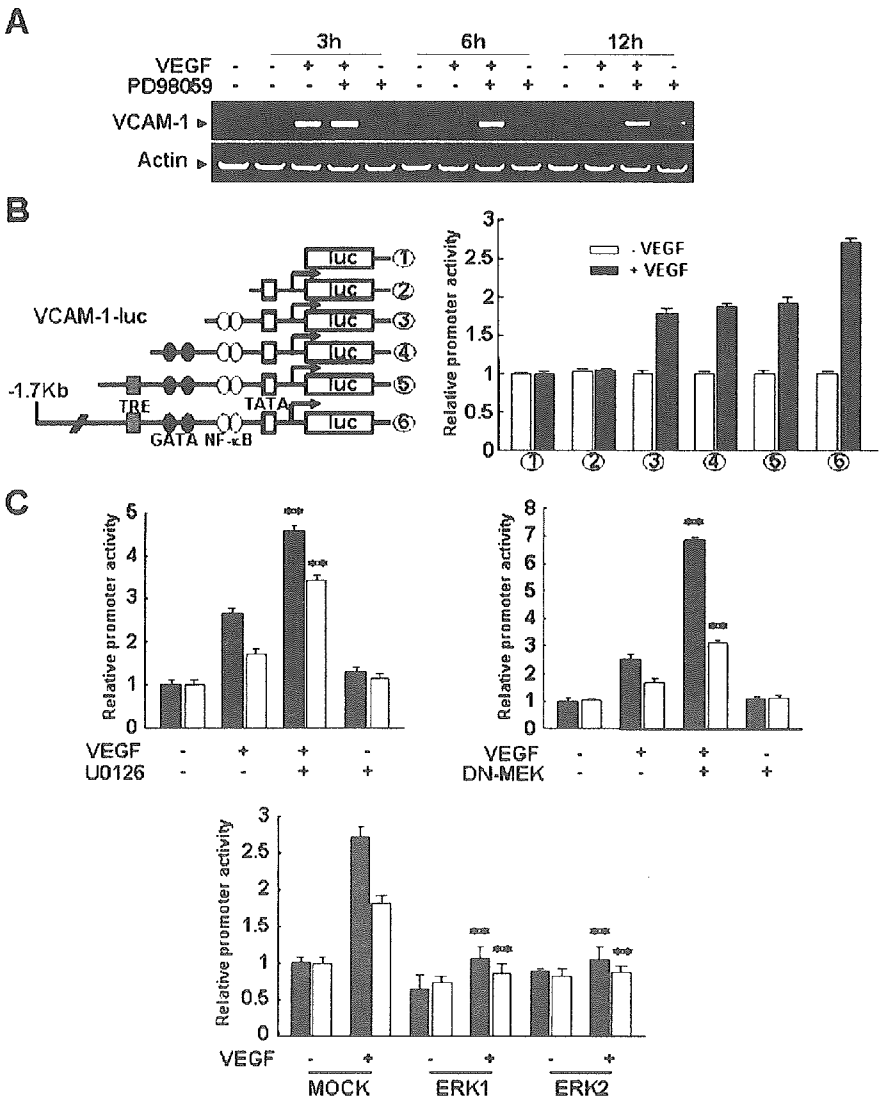

Fig. 2. ERK down-regulates VEGF-induced transcription of VCAM-1 by inhibiting NF-κB. (A) HUVECs were incubated for 30 min with or without 10 μM PD98059 and stimulated with 10 ng/ml VEGF for the indicated times. Total mRNAs were isolated and RT-PCR was performed with specific primers for human VCAM-1 as described in "Materials and methods". Actin served as an internal control. (B) HUVECs were cotransfected with a β-galactosidase plasmid and the various pVCAM-1-Luc deletion constructs as depicted. Twenty four hours later they were stimulated with 10 ng/ml VEGF for 24 h. (C) HUVECs were cotransfected with pVCAM-1-Luc (fragment 6: 1.8 kilobase pair, fragment 3: 329 bp), a β-galactosidase plasmid, and a dominant negative form of MEK1 (DN-MEK1), or wild form of ERKs (ERK1, 2). Twenty four hours after transfection, they were incubated with 10 ng/ml VEGF for 24 h. Luciferase activity was normalized to β-galactosidase activity. Data are means ± S.D. of luciferase light units relative to control untreated cells (set at 100%) in quadruplicate experiments. **, $P < 0.01$ versus VEGF alone or MOCK + VEGF.

chemiluminescent reagent as recommended by Amersham Biosciences, Inc.

2.13. Statistical analysis

Data are presented as means±S.E, and statistical comparisons between groups were performed by 1-way ANOVA followed by Student's *t* test.

3. Results

3.1. Inhibition of ERK resulted in increased expression of VCAM-1 in response to VEGF

Vascular endothelial growth factor (VEGF), a well characterized angiogenic factor, also acts as a proinflammatory cytokine that produces enhanced leukocyte rolling and adhesion and increases endothelial permeability [29,30]. In endothelial cells, it strongly activates ERK and also induces expression of CAMs [31,32] in a NF-κB-dependent mechanism [31]. However, the level of CAM induction in response to VEGF is significantly lower, when compared in parallel, than those by TNF-α and IL-β, which show very little or negligible effect on ERK activation in endothelial cells (data not shown). Thus, it is supposed that the ERK pathway may interfere expression of inflammatory CAMs in response to proinflammatory factors in endothelium. To test this possibility, we first evaluated the role of ERK in VEGF-induced expression of inflammatory response gene such as VCAM-1 by employing MEK inhibitors, PD98059 and U0126, in endothelial cells. Treatment of HUVECs with VEGF enhanced VCAM-1 expression, with a maximum at 8 h (Fig. 1A). In the presence of 5 μM U0126, the effect of VEGF was markedly increased and prolonged up to 24 h (Fig. 1A). To confirm this inhibitory effect, we treated HUVECs with VEGF

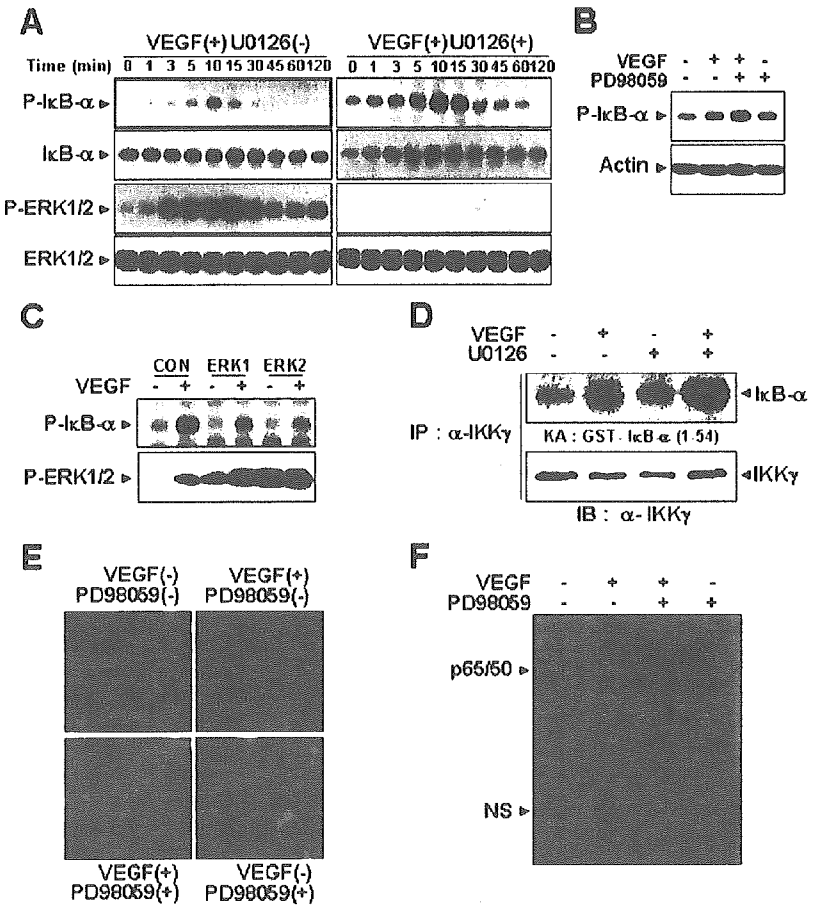

Fig. 3. Inhibition of ERK increases VEGF-induced IKK activity and nuclear translocation of NF-κB. (A) HUVECs were preincubated for 30 min with or without 5 μM U0126 and then stimulated with 10 ng/ml VEGF for the indicated times. Western blots were probed with anti-phospho-IκBα, anti-IκBα, anti-phospho-ERK, and anti-ERK antibodies. (B) HUVECs were preincubated for 30 min with or without 10 μM PD98059 and then stimulated with 10 ng/ml VEGF for 10 min. Western blots were probed with anti-phospho-IκBα and reprobed with an anti-actin antibody to verify equal loading of protein in each. (C) HUVECs were transfected with ERKs wild form (ERK1, 2) and then stimulated with VEGF for 10 min. Western blots were probed with anti-phospho-IκBα, and anti-phospho-ERK antibodies. (D) IKK activity was assessed by immune complex kinase assay as described in "Materials and methods". Recovery of IKK was assessed by immunoblotting for IKK-γ. (E) Immunocytochemical analysis of p65 localization. HUVECs were preincubated for 30 min with or without 10 μM PD98059 and then stimulated with 10 ng/ml VEGF for 30 min and subjected to immunocytochemistry as described in "Materials and methods". (F) HUVECs were preincubated for 30 min with or without 10 μM PD98059 and then stimulated with VEGF (20 ng/ml) for 30 min. Nuclear extracts were isolated and gel shift assay performed with a ^{32}P-radiolabeled NF-κB oligonucleotide of human VCAM-1.

for 10 min in the presence or absence of 5 μM U0126 and measured ERK activity by Western blotting with antibody against the phosphorylated form of ERK1/2 (p44 ERK1 and p42 ERK2). As shown in Fig. 1B, U0126 completely inhibited VEGF-induced ERK activation, whereas VEGF-induced VCAM-1 expression was increased (Fig. 1B). Pretreatment with the other MEK inhibitor, PD98059, also augmented VEGF-induced VCAM-1 expression, while reducing ERK activation (Fig. 1B). U0126 or PD98059 alone had no effect on VCAM-1 expression (Fig. 1B). In addition, the U0126-induced increase in VEGF-induced VCAM-1 expression was dose-dependent, and inversely related to ERK activity (Fig. 1C). FACScan analysis confirmed that U0126 augmented VEGF-induced expression of VCAM-1 on the cell surface of HUVECs (Fig. 1D).

To further confirm that the enhancement of VEGF-induced VCAM-1 expression by the inhibitors was due specifically to inhibition of ERK signaling, we determined the effects of a dominant negative MEK1 (DN-MEK1) mutant and two types of wild type ERK (ERK1 and ERK2). In agreement with the results with chemical inhibitors, Western blot analysis showed that overexpression of DN-MEK1 reduced VEGF-induced ERK phosphorylation, and increased the induction of VCAM-1 by VEGF (Fig. 1E). Moreover, there was a small increase in basal VCAM-1 expression in the cells expressing DN-MEK-1 (Fig. 1E). In contrast, HUVECs overexpressed with either wild type ERK1 or ERK2 increased ERK phosphorylation, and decreased VCAM-1 expression in response to VEGF (Fig. 1F). These results confirm that the ERK pathway inhibits VEGF signaling leading to VCAM-1 expression in endothelial cells.

3.2. ERK down-regulates VEGF-induced transcription of VCAM-1 by inhibiting NF-κB

To determine whether ERK inhibits VEGF-activated transcription of VCAM-1 in endothelial cells, we performed semi-quantitative RT-PCR and assayed transcription from the VCAM-1 luciferase plasmids described in Materials and methods. Treatment of HUVECs with VEGF in the absence of ERK inhibitor induced the appearance of VCAM-1 mRNA within 3 h, and the mRNA declined thereafter (Fig. 2A). In the presence of 10 μM PD98059, the level of VCAM-1 mRNA induced by VEGF was increased and sustained up to 12 h (Fig. 2A). These changes could result either from new synthesis or from increased mRNA stability. Pretreatment with actinomycin D, an inhibitor of transcription, almost completely prevented the increase of VCAM-1 mRNA in response to PD98059 (data not shown), suggesting that ERK inhibits VEGF-activated transcription. The human VCAM-1 promoter (1.7 kb) includes binding sites for NF-κB, TRE, and GATA [26]. Although previous report have implicated NF-κB in VEGF-induced VCAM-1 expression in endothelial cells [26,33], its precise role in activation of the VCAM-1 promoter has not been determined. To identify the cis elements involved, we serially deleted the 1.7 kb VCAM-1 promoter and introduced the resulting plasmids into HUVECs. As shown in Fig. 2B, deletion of the 5′ 1.2 kb region substantially reduced the response to VEGF, but further deletion of the TRE and GATA sites had no appreciable effect. Deletion of the proximal NF-κB binding sites located about 65 and 75 bp upstream of the transcription start site resulted in complete lose of responsiveness to VEGF. These results demonstrate that the NF-κB motifs on the VCAM-1 promoter are important for VEGF-mediated activation of the VCAM-1 promoter, together with an unidentified element in the 5′ 1.2 kb upstream region.

To further confirm the role of ERK in VEGF-induced VCAM-1 transcription, HUVECs were transiently transfected with a VCAM-1 luciferase plasmid harboring the VCAM-1 promoter region. As shown in Fig. 2C, VEGF induced VCAM-1-dependent transcriptional activity, and this was increased by pretreatment with 5 μM U0126, or by introducing DN-MEK-1, but abrogated by ERK or ERK2. These results confirm that ERK controls VEGF-mediated expression of VCAM-1 at the transcriptional level. Since the NF-κB motifs play a significant role in VEGF-induced transcription of VCAM-1, it seemed possible that ERK suppressed activation of NF-κB by VEGF. Indeed, VEGF-induced transcription from a luciferase plasmid containing the proximal NF-κB binding sites of the VCAM-1 promoter was markedly increased by U0126 and DN-MEK1, and almost completely blocked by ERK1 or ERK2 (Fig. 2C). These results suggest that ERK inhibits VEGF-induced transcription of VCAM-1 mRNAs at least in part by suppressing transcription from the NF-κB elements in the VCAM-1 promoter.

3.3. Inhibition of ERK increases VEGF-induced IKK activity and nuclear translocation of NF-κB

The activated form of NF-κB is a heterodimer that usually consists of two proteins, a p65 (also called relA) subunit and a

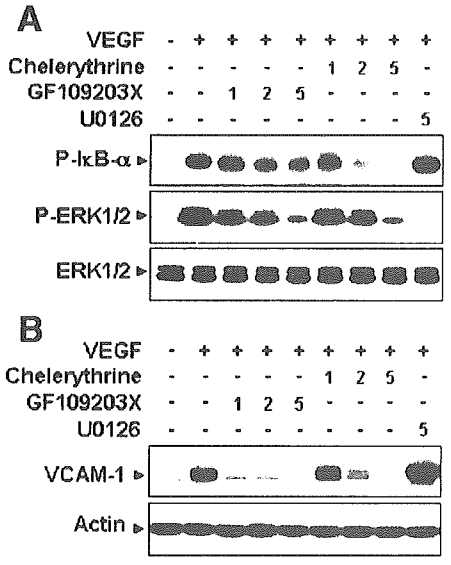

Fig. 4. PKC mediates both IκBα phosphorylation and ERK activation by VEGF. HUVECs were preincubated for 30 min with or without GF109203X, chelerythrine chloride (1, 2, or 5 μM) or 5 μM U0126 and then stimulated with 10 ng/ml VEGF for 10 min (A) or 8 h. (B). Western blots were probed with anti-phospho-IκBα, anti-IκBα, anti-phospho-ERK, and anti-ERK antibodies (A), and anti-VCAM-1 and anti-actin antibodies (B). Actin was used to verify equal loading of protein.

p50 subunit [7]. In the inactive state, NF-κB is found in the cytoplasm bound to IκBα, which prevents it from entering the nuclei [7,34]. Activation of NF-κB is preceded by the phosphorylation, ubiquitination, and proteolytic degradation of IκBα [34]. Therefore, we examined the effect of ERK inhibitors on VEGF-induced IκBα phosphorylation and degradation by Western blotting with antibodies against phospho-IκBα (Ser-32) and IκBα. As shown in Fig. 3A, VEGF treatment led to phosphorylation of IκBα and maximal activation was observed after 10 min. Pretreatment with U0126 substantially enhanced VEGF-induced IκBα phosphorylation. Moreover, while degradation of IκBα was barely detectable after stimulation with VEGF on its own, when U0126 was added, the level of IκBα markedly decreased following 30 min of VEGF treatment (Fig. 3A). We also observed that PD98059 increased the effect of VEGF on phosphorylation and subsequent degradation of IκBα in a manner similar to U0126 (Fig. 3B). In contrast, VEGF-induced IκBα phosphorylation was almost completely abrogated by overexpression of ERK1 or ERK2 (Fig. 3C). To further confirm the effect of U0126 on VEGF-induced IκBα phosphorylation, the IκB kinase (IKK) enzymatic assay was performed. IKK is a complex composed of three subunits: IKKα (IKK1), IKKβ (IKK2), and IKKγ (NEMO, IKKAP) [11]. IKK activity was determined in anti-IKKγ

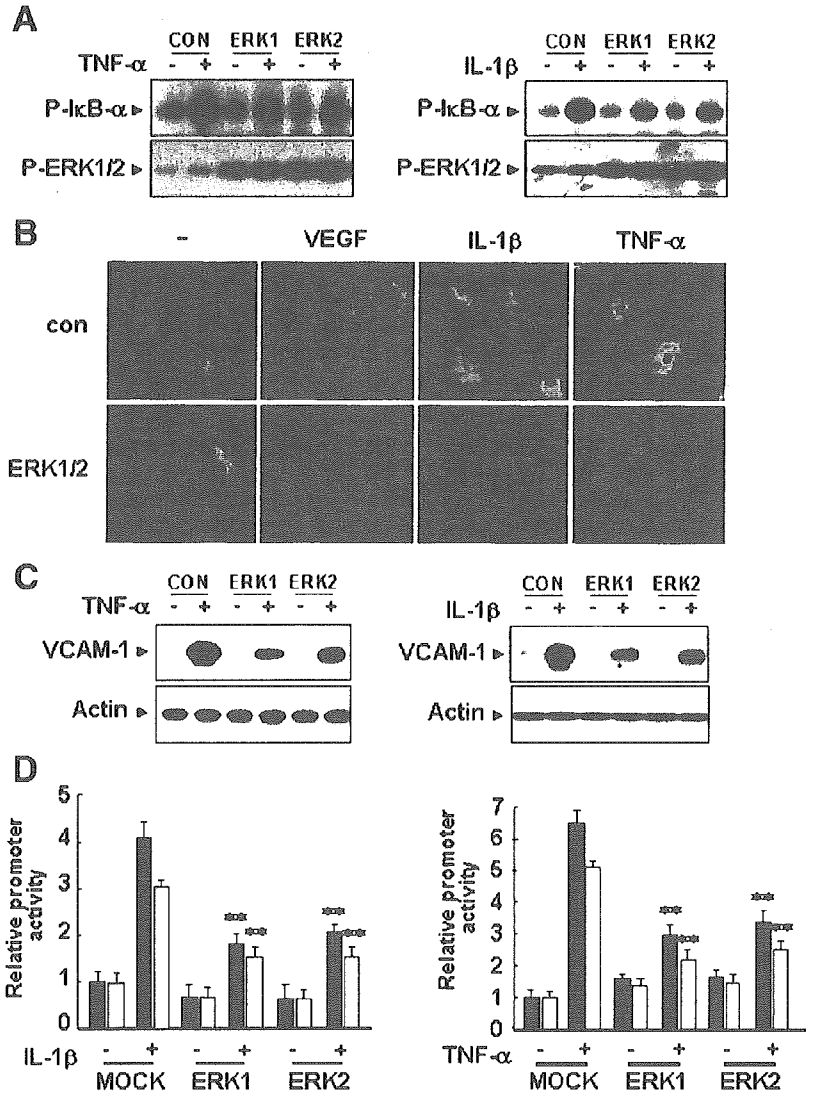

Fig. 5. Overexpression of ERK suppresses NF-κB activation and VCAM-1 expression in response to IL-1β and TNF-α. (A) HUVECs were transfected with ERK wild form (ERK1, 2) and then stimulated with 10 ng/ml TNF-α or 50 units/ml IL-1β for 10 min. Western blots were probed with anti-phospho-IκBα and anti-phospho-ERK antibodies. (B) Immunocytochemical analysis of p65 localization. HUVECs were transfected with ERKs wild form (ERK1, 2) and then stimulated with 10 ng/ml VEGF, 10 ng/ml TNF-α or 50 units/ml IL-1β for 30 min and subjected to immunocytochemistry as described in "Materials and methods". (C) HUVECs were transfected with ERKs wild form (ERK1, 2) and then stimulated with 10 ng/ml TNF-α or 50 units/ml IL-1β for 8 h. Western blots were probed with anti-VCAM-1 and reprobed with an anti-actin antibody to verify equal loading of protein in each. (D) HUVECs were cotransfected with pVCAM-1-Luc (fragment 6: 1.8 kilobase pair, fragment 3: 329 bp), a β-galactosidase plasmid, and a ERKs wild form (ERK1, 2). Twenty four hours after transfection, they were incubated with 10 ng/ml TNF-α or 50 units/ml IL-1β for 24 h. Luciferase activity was normalized to β-galactosidase activity. Data are means±S.D. of luciferase light units relative to control untreated cells (set at 100%) in quadruplicate experiments. **, $P<0.01$ versus MOCK+IL-1β or MOCK+TNF-α.

immunoprecipitates as described [28]. Cell stimulation with VEGF activated the ability of IKK to phosphorylate GST-IκBα (Fig. 3D). This VEGF-induced IKK activation was significantly increased by pretreatment of U0126 (Fig. 3D).

The dissociation of NF-κB from IκBα results in translocation of NF-κB to the nucleus, where it binds to specific sequences in the promoter regions of target genes. We next determined the effect of ERK inhibitors on VEGF-induced nuclear translocation and NF-κB DNA binding activity. VEGF caused nuclear translocation of the p65 subunit of NF-κB and this was significantly increased by pretreatment with PD98059 (Fig. 3E). Furthermore binding to target NF-κB oligonucleotides was also markedly augmented by pretreatment with PD98059 (Fig. 3F). PD98059 on its own had no effect on nuclear translocation and NF-κB DNA binding activity (Fig. 3E and F). Collectively, these results suggest that ERK suppresses VEGF-induced NF-κB activation by blocking the VEGF signaling pathway leading to IκBα phosphorylation.

3.4. PKC mediates both IκBα phosphorylation and ERK activation by VEGF

Our data indicate that VEGF induces both IκBα phosphorylation and ERK activation in endothelial cells. It was of interest to identify the upstream signaling molecules that lead to IKK and ERK activation. A previous study suggested the involvement of PKC in NF-κB activation leading to endothelial CAM expression [31,35,36]. We therefore examined the role of PKC in IκBα phosphorylation by employing two PKC inhibitors, GF109203X and chelerythrine chloride, and, in parallel, compared the effect of these inhibitors on VEGF-induced ERK activation. As shown in Fig. 4A, both IκBα phosphorylation and ERK activation in response to VEGF were inhibited by GF109203X and chelerythrine chloride, indicating that PKC lies upstream of both IKK and ERK. Under the same condition, U0126 completely inhibited ERK activation in response to VEGF, and increased the VEGF effect on IκBα phosphorylation (Fig. 4A). Similarly, VEGF-induced VCAM-1 expression was blocked by GF109203X and chelerythrine chloride, but increased by U0126 (Fig. 4B). These results suggest that in the VEGF signaling pathway PKC provides a positive signal activating IKK and ERK, a negative signal.

3.5. Overexpression of ERK suppresses NF-κB activation and VCAM-1 expression in response to IL-1β and TNF-α

The role of ERK pathway in other cytokine-induced NF-κB activation was explored. Unlikely to VEGF, IL-1β and TNF-α did not significantly induce ERK activation in HUVECs in contrast to their strong stimulatory activity on NF-κB. Consistently, inhibition of ERK by pretreatment of HUVECs with 5 μM U0126 did not further increase IκBα phosphorylation in response to either IL-1β or TNF-α (data not shown). However, overexpression of either wild type ERK1 or ERK2 markedly reduced both IL-1β-and TNF-α-induced IκBα phosphorylation (Fig. 5A). In addition, nuclear translocation of

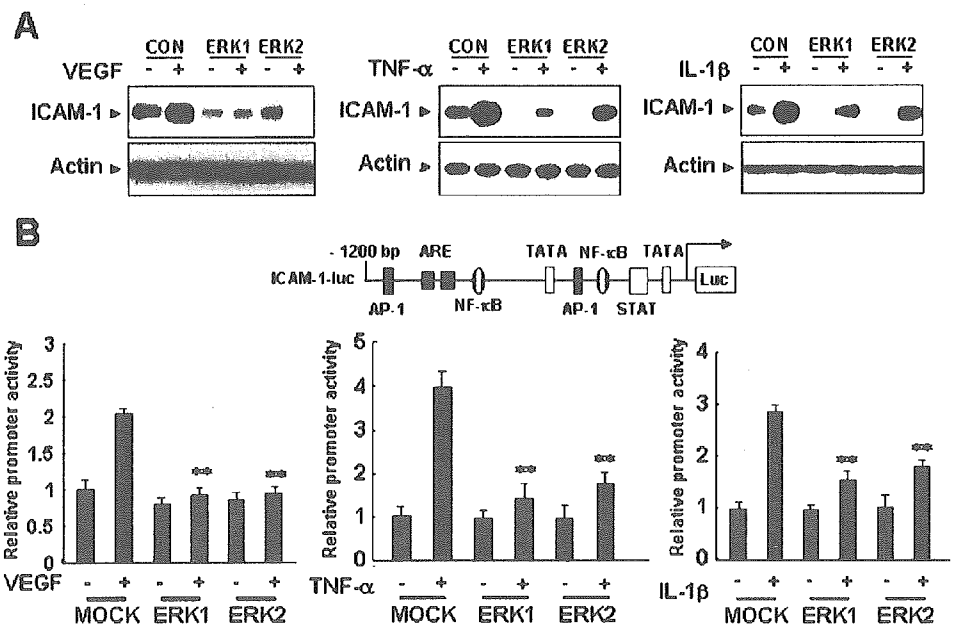

Fig. 6. ERK reduces endothelial ICAM-1 expression in response to VEGF, IL-1β, and TNF-α. (A) HUVECs were transfected with ERKs wild form (ERK1, 2) and then stimulated with 10 ng/ml VEGF, 10 ng/ml TNF-α or 50 units/ml IL-1β for 8 h. Western blots were probed with anti-ICAM-1 and reprobed with an anti-actin antibody to verify equal loading of protein in each. (B) HUVECs were cotransfected with pICAM-1-Luc (1.2 kilobase pair), a β-galactosidase plasmid, and a ERKs wild form (ERK1, 2). Twenty four hours after transfection, they were incubated with 10 ng/ml VEGF, 10 ng/ml TNF-α or 50 units/ml IL-1β for 24 h. Luciferase activity was normalized to β-galactosidase activity. Data are means±S.D. of luciferase light units relative to control untreated cells (set at 100%) in quadruplicate experiments. **, $P<0.01$ versus MOCK+VEGF, MOCK+IL-1β or MOCK+TNFα.

p65 subunit of NF-κB induced by either IL-1β or TNF-α was blocked by overexpression of ERKs (Fig. 5B). In agreement, both IL-1β and TNF-α increased endothelial VCAM-1 expression in a NF-κB dependent manner as shown in a promoter assay and these responses were significantly abrogated by overexpression of either ERK1 or ERK2 (Fig. 5C and D). These results raised the possibility that ERK negatively regulates NF-κB-dependent gene expression in endothelial cells through inhibiting the IκBα phosphorylation pathway stimulated by various agonists.

3.6. ERK reduces endothelial ICAM-1 expression in response to VEGF, IL-1β, and TNF-α

We further confirmed the role of ERK pathway on expression of other inflammatory genes in endothelial cells. ICAM-1 is one of representative endothelial cell adhesion molecules expressed in a NF-κB dependent mechanism. As expected, the protein level of ICAM-1 on HUVECs was increased by either treatment of VEGF, IL-1β or TNF-α (Fig. 6A). All these increases were almost completely or markedly

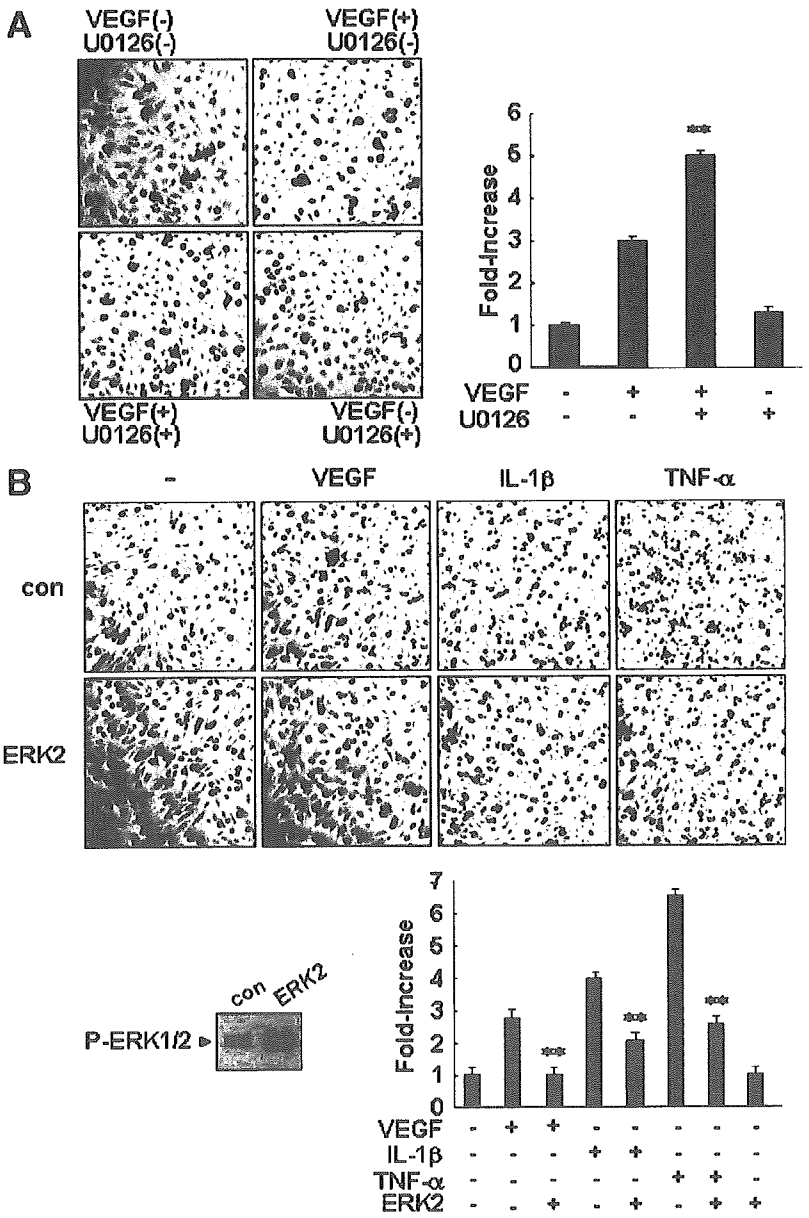

Fig. 7. ERK inhibitors increase VEGF-Induced leukocyte adhesion to endothelial cells. (A) HUVECs were preincubated for 30 min with or without 5 μM U0126 and then stimulated with 10 ng/ml VEGF for 8 h. (B) ERK2 lentiviral vectors were added to cell cultures at varying multiplicities of infection (MOIs ≈1–50). At 18 h, cells were washed and medium was replaced. HUVECs were stimulated with 10 ng/ml VEGF, 10 ng/ml TNF-α or 50 units/ml IL-1β for 8 h. Thereafter adhesion to U937 human monocytes was measured as described in "Materials and methods." Data are means±S.D. of adhesion relative to control untreated cells (set at 100%) in quadruplicate experiments. **, $P<0.01$ versus VEGF, IL-1β or TNF-α.

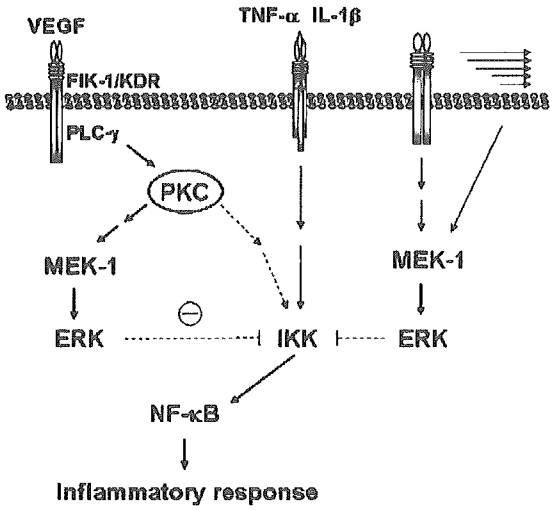

Fig. 8. Potential mechanism supporting anti-inflammatory role of ERK in the vascular wall.

inhibited by overexpression of either ERK1 or ERK2 (Fig. 6A). Consistently, ICAM-1-dependent transcriptional activities induced by these cytokines were inhibited by overexpression of ERK1 or ERK2 (Fig. 6B).

3.7. ERK inhibitors increase VEGF-Induced leukocyte adhesion to endothelial cells

Expression of CAMs, such as ICAM-1 and VCAM-1, on the surface of endothelial cells is required for endothelial–leukocyte interaction. Since inhibition of the ERK pathway increases the effect of VEGF on endothelial CAM expression, we tested whether the ERK inhibitor stimulates leukocyte adhesion to endothelial cells. HUVECs were exposed to 10 ng/ml VEGF for 8 h and then co-cultured with human monocytic U937 cells for an additional 1 h. As shown in Fig. 7, the adhesion of U937 cells to HUVECs was increased by VEGF, and this effect was accentuated by pretreatment with 5 μM U0126 (Fig. 7A). U0126 alone, on the other hand, had no effect (Fig. 7A). In contrast, overexpression of ERK2 markedly reduced VEGF-induced adhesion of U937 cells to HUVECs (Fig. 7B). Moreover, both IL-1β-and TNF-α-induced monocyte–endothelial cell interaction was also significantly reduced by overexpression of ERK2 (Fig. 7B). 4.

4. Discussion

Unveiling of endothelial NF-κB activation is pivotal for understanding the inflammatory reaction and the pathogenesis of inflammatory vascular diseases. A large number of studies have revealed the presence of a number of cellular stimuli, including inflammatory cytokines and oscillating shear stress, that lead to the endothelial NF-κB activation [10,37]. Conversely, factors such as angiopoietin-1, bFGF, hepatocyte growth factor (HGF), and normal lamina shear stress were shown to suppress NF-κB activation [38,39]. However, despite of a number of reports, precise understanding of their action mechanisms in the vasculature remains still unclear. Importantly, the present study demonstrates the novel role of ERK in controlling endothelial NF-κB activation and inflammatory gene expression.

Our data showed that inhibition of ERK increased VCAM-1 expression in response to VEGF stimulation, but that ERK inhibitors alone had no significant effect. This indicates that inhibition of ERK itself is incapable of stimulating VCAM-1 expression in endothelial cells, and suggests that VEGF sets in train both positive and negative signals related to VCAM-1 expression and that ERK may serve as an internal suppressor of the positive signal. Using two PKC inhibitors, it is clearly demonstrated that VEGF stimulates both ERK and IKK through PKC that lies downstream of KDR/Flk. Since ERK inhibits IKK activation by VEGF (Fig. 4), PKC seems to transmit both positive and negative signals involved in IKK activation. Therefore, the relatively weak activation of IKK and expression of inflammatory genes by VEGF is likely to be due to the concomitant activation of ERK. Similar phenomenon was observed in TNF-related activation-induced cytokine (TRANCE)-induced NF-κB activation and VCAM-1 expression. TRANCE stimulated ERK, IκBα phosphorylation, and transcriptional activity of NF-κB in HUVECs [40,41]. Pretreatment of the ERK inhibitors significantly enhanced TRANCE-induced NF-κB activation and VCAM-1 expression (data not shown), suggesting the suppressive role of concomitantly activated ERK in the cytokine-induced NF-κB pathway in endothelial cells.

Unlikely to VEGF, IL-1β and TNF-α had little effect on ERK activation in HUVECs, but they much strongly induced IKK activation and VCAM-1 expression compared to VEGF. The effects of IL-1β and TNF-α on IKK activation and VCAM-1 expression was very slightly increased by the ERK inhibitor (data not shown) but markedly suppressed by overexpression of ERK1 or ERK2. We also tested the effect of bFGF and EGF on VCAM-1 expression in HUVECs. These two growth factors markedly stimulated ERK activation in HUVECs, but did not induce VCAM-1 expression. In addition, ERK inhibitors had no significant effect on VCAM-1 expression (data not shown), presumably because these growth factors do not activate the NF-κB signaling pathway. We have recently reported that HGF counteracts VEGF-induced endothelial CAM expression through inhibiting IKK-mediated NF-κB activation [42]. HGF itself was unable to induce NF-κB activation but strongly stimulated ERK activation in endothelial cells (data not shown). In deed, it is observed that pretreatment of the ERK inhibitor prior to HGF administration results in reversing the inhibitory effect of HGF on VEGF-induced IκBα phosphorylation and VCAM-1 expression (data not shown). Although the precise mechanism engaged in agonists-dependent activation or inhibition of NF-κB pathway remains elusive, it is at least in part suggested that the cellular level of ERK activity may be one of crucial components to control IKK-mediated NF-κB activation in endothelial cells. Western blotting with antibodies against phospho-IκBα (Ser-32) and IκBα revealed that the ERK inhibitors increase IκBα phosphorylation at Ser-32 and degradation in response to VEGF (Fig. 4). Conversely, forced elevation of ERK activity in HUVECs resulted in the

inhibition of phosphorylation of IκBα on Ser-32 by VEGF, IL-1β, and TNF-α. IKK exists as a high molecular complex containing two kinase subunits, IKKα (IKK1) and IKKβ (IKK2), and a regulatory subunit, NEMO [13]. The phosphorylation of IκBα on Ser-32 and Ser-36 is mediated mainly by the kinase activity of IKKβ and led to its proteolytic degradation and subsequent nuclear translocation of NF-κB [13]. Therefore, ERK is most likely to inhibit the canonical NF-κB pathway that involves IKK-mediated IκBα phosphorylation in endothelial cells.

In conclusion, our present data apparently demonstrate a novel function of ERK as a curb of endothelial NF-κB activation with possible mechanism (Fig. 8). Indeed, elevation of ERK activity in endothelial cells significantly suppressed expression of NF-κB-dependent genes such as ICAM-1 and VCAM-1 in response to cytokine stimulation. These effects were functionally correlated with decreased endothelial cell–monocyte interaction. Although the further study is required to prove the anti-inflammatory nature of ERK in more complex in vivo environment, our findings suggest that ERK activity constitutively or transiently induced by normal laminar flow or various endothelial stimuli may serve as a negative regulator of vascular inflammation by suppressing endothelial NF-κB activation. Therefore, measuring the existence of ERK activity in vascular endothelial cells may be useful for predicting the feasibility and potency of inflammatory reactions in the vascular wall.

Acknowledgments

This work was supported by a Next Generation Growth Engine Program Grant and Vascular System Research Center Grant from the Korean Ministry of Science and Technology.

References

[1] H. Ulbrich, E.E. Eriksson, L. Lindbom, Trends Pharmacol. Sci. 24 (2003) 640.
[2] D. Vestweber, Curr. Opin. Cell Biol. 14 (2002) 587.
[3] W.A. Muller, Lab Invest. 82 (2002) 521.
[4] P. Xia, J.R. Gamble, K.A. Rye, L. Wang, C.S. Hii, P. Cockerill, Y. Khew-Goodall, A.G. Bert, P.J. Barter, M.A. Vadas, Proc. Natl. Acad. Sci. U. S. A. 95 (1998) 14196.
[5] K.T. Piercy, R.L. Donnell, S.S. Kirkpatrick, C.H. Timaran, S.L. Stevens, M.B. Freeman, M.H. Goldman, J. Surg. Res. 105 (2002) 215.
[6] S. Zeuke, A.J. Ulmer, S. Kusumoto, H.A. Katus, H. Heine, Cardiovasc. Res. 56 (2002) 126.
[7] J. Peter, D.M. Barnes, Sc. D, Michael Karin, N. Engl. J. Med. 336 (1997) 1066.
[8] P.A. Baeuerle, T. Henkel, Annu. Rev. Immunol. 12 (1994) 141.
[9] C. Maaser, S. Schoeppner, T. Kucharzik, M. Kraft, E. Schoenherr, W. Domschke, N. Luegering, Clin. Exp. Immunol. 124 (2001) 208.
[10] J.T. Wu, J.G. Kral, J. Surg. Res. 123 (2005) 158.
[11] Y. Yamamoto, R.B. Gaynor, Trends Biochem. Sci. 29 (2004) 72.
[12] P. Viatour, M.P. Merville, V. Bours, A. Chariot, Trends Biochem Sci. 30 (2005) 43.
[13] M.S. Ayden, S. Hosh, Genes Dev. 18 (2004) 2195.
[14] E. Majewska, E. Paleolog, Z. Baj, U. Kralisz, M. Feldmann, H. Tchorzewski, Scand. J. Immunol. 45 (1997) 385.
[15] H. Zhang, A.C. Issekutz, Am. J. Pathol. 160 (2002) 2219.
[16] M. Kaneki, S. Kharbanda, P. Pandey, K. Yoshida, M. Takekawa, J.R. Liou, R. Stone, D. Kufe, Mol. Cell. Biol. 19 (1999) 461.
[17] R. Datta, K. Yoshinaga, M. Kaneki, P. Pandey, D. Kufe, J. Biol. Chem. 275 (2000) 41000.
[18] J.H. Je, J.Y. Lee, K.J. Jung, B. Sung, E.K. Go, B.P. Yu, H.Y. Chung, FEBS Lett. 566 (2004) 183.
[19] C. Schmidt, B. Peng, Z. Li, G.M. Sclabas, S. Fujioka, J. Niu, M. Schmidt-Supprian, D.B. Evans, J.L. Abbruzzese, P.J. Chiao, Mol. Cell. 12 (2003) 1287.
[20] J.R. Burke, J. Strnad, Biochem. Biophys. Res. Commun. 293 (2002) 1508.
[21] P.E. Hughes, M.W. Renshaw, M. Pfaff, J. Forsyth, V.M. Keivens, M.A. Schwartz, M.H. Ginsberg, Cell 88 (1997) 521.
[22] R. Gum, H. Wang, E. Lengyel, J. Juarez, D. Boyd, Oncogene 14 (1997) 481.
[23] D. Besser, M. Presta, Y. Nagamine, Cell Growth Differ. 6 (1995) 1009.
[24] E. Meylan, F. Martinon, M. Thome, M. Gschwendt, J. Tschopp, EMBO Rep. 3 (2002) 1201.
[25] E.A. Jaffe, R.L. Nachman, C.G. Becker, C.R. Minick, J. Clin. Invest. 52 (1973) 2745.
[26] T. Minami, W.C. Aird, J. Biol. Chem. 276 (2001) 47632.
[27] D. Cefai, E. Simeoni, K.M. Ludunge, R. Driscoll, L.K. von Segesser, L. Kappenberger, G. Vassalli, J. Mol. Cell. Cardiol. 38 (2005) 333.
[28] Y. Takada, A. Mukhopadhyay, G.C. Kundu, G.H. Mahabeleshwar, S. Singh, B.B. Aggarwal, J. Biol. Chem. 278 (2003) 24233.
[29] M.A. Proescholdt, S. Jacobson, N. Tresser, E.H. Oldfield, M.J. Merrill, J. Neuropathol. Exp. Neurol. 61 (2002) 914.
[30] S.D. Croll, J.H. Goodman, H.E. Scharfman, Adv. Exp. Med. Biol. 548 (2004) 57.
[31] I. Kim, S.O. Moon, S.H. Kim, H.J. Kim, Y.S. Koh, G.Y. Koh, J. Biol. Chem. 276 (2001) 7614.
[32] I. Kim, S.O. Moon, S.K. Park, S.W. Chae, G.Y. Koh, Circ. Res. 89 (2001) 477.
[33] H.J. Park, Y.W. Lee, B. Hennig, M. Toborek, Nutr. Cancer 41 (2001) 126.
[34] V. Dixit, T.W. Mak, Cell 111 (2002) 615.
[35] K. Page, J. Li, L. Zhou, S. Iasvovskaia, K.C. Corbit, J.W. Soh, I.B. Weinstein, A.R. Brasier, A. Lin, M.B. Hershenson, J. Immunol. 170 (2003) 5681.
[36] T. Minami, M.R. Abid, J. Zhang, G. King, T. Kodama, W.C. Aird, J. Biol. Chem. 278 (2003) 6976.
[37] G.P. Sorescu, M. Sykes, D. Weiss, M.O. Platt, A. Saha, J. Hwang, N. Boyd, Y.C. Boo, J.D. Vega, W.R. Taylor, H. Jo, J. Biol. Chem. 278 (2003) 31128.
[38] E. Eng, B.J. Ballermann, Microvasc. Res. 65 (2003) 137.
[39] B.H. Jeon, F. Khanday, S. Deshpande, A. Haile, M. Ozaki, K. Irani, Circ. Res. 92 (2003) 586.
[40] Y.M. Kim, Y.M. Kim, Y.M. Lee, H.S. Kim, J.D. Kim, Y. Choi, K.W. Kim, S.Y. Lee, Y.G. Kwon, J. Biol. Chem. 277 (2002) 6799.
[41] J.K. Min, Y.M. Kim, S.W. Kim, M.C. Kwon, Y.Y. Kong, I.K. Hwang, M. H. Won, J. Rho, Y.G. Kwon, J. Immunol. 175 (2005) 531.
[42] J.K. Min, Y.M. Lee, J.H. Kim, Y.M. Kim, S.W. Kim, S.Y. Lee, Y.S. Gho, G.T. Oh, Y.G. Kwon, Circ. Res. 96 (2005) 300.

Enhanced Functional Gap Junction Neoformation by Protein Kinase A–Dependent and Epac-Dependent Signals Downstream of cAMP in Cardiac Myocytes

Satoshi Somekawa, Shigetomo Fukuhara, Yoshikazu Nakaoka, Hisakazu Fujita, Yoshihiko Saito, Naoki Mochizuki

Abstract—Gap junctions (GJs) constituted by neighboring cardiac myocytes are essential for gating ions and small molecules to coordinate cardiac contractions. cAMP is suggested to be a potent stimulus for enhancement of GJ function. However, it remains elusive how cAMP potentiates the GJ of cardiomyocytes. Here we demonstrated that the gating function of GJ is enhanced by the protein kinase A (PKA)–dependent signal, and that the accumulation of connexin43 (Cx43), the most abundant Cx in myocytes, is enhanced by an exchange protein directly activated by cAMP (Epac) (Rap1 activator)–dependent signal. The gating function of GJs was analyzed by microinjected dye transfer method. The accumulation of Cx43 was analyzed by quantitative immunostaining. Using the PKA-specific activator N^6-benzoyladenosine-3′,5′-cyclic monophosphate (6Bnz) and Epac-specific activator 8-(4-chlorophenylthio)-2′-*O*-methyladenosine-3′,5′-cyclic monophosphate (8CPT), we could delineate the two important downstream signals of cAMP for enhanced GJ neoformation. Whereas 6Bnz potentiated gating function of GJs with slight accumulation of Cx43 at cell–cell contacts, 8CPT remarkably enhanced the accumulation of Cx43 with a slight effect on gating. We further noticed that adherens junctions (AJs) were maturated by 8CPT, as marked by increased neural-cadherin immunostaining. Because AJ formation precedes the GJ formation, AJ formation accelerated by Epac-Rap1 signal may result in enhanced GJ formation. The involvement of Epac-Rap1 signal in GJ neoformation was further confirmed by evidence that inactivation of Rap1 by overexpression of Rap1GAP1b perturbed the accumulation of Cx43 at cell–cell contacts. Collectively, PKA and Epac cooperatively enhance functional GJ neoformation in cardiomyocytes. (***Circ Res.* 2005;97:655-662.**)

Key Words: gap junction ■ connexin43 ■ myocardial structure ■ cardiac gap junction connexins

Gap junctions (GJs) are channels formed by two docking connexons; one connexon is provided by each of the two contiguous cells and is constituted of six connexin (Cx) molecules.[1] Among the 20 Cx members, Cx40, Cx43, and Cx45 are expressed in the heart.[2] Of the three, Cx43 is predominantly expressed in working heart muscle cells.[3,4] GJs in the heart are characterized by their localization at the intercalated disk between each myocyte and also by their role in electrical conductance required for coordinated electrical excitation.[5] Myocytes electrically coupled by GJs show synchronized contraction. The importance of Cx43 in electrical excitation in vivo is evident by cardiac-specific depletion of Cx43 leading to cardiac arrhythmia.[6]

The overall function of GJs depends on the number of GJs and the gating function of assembled GJs. GJs are upregulated by increased transcription of Cx, increased distribution of Cx at cell–cell contacts, and decreased degradation of Cx from the cell membrane. cAMP increases Cx43 mRNA.[7] cAMP also enhances the trafficking of Cx43 from the endoplasmic reticulum/Golgi apparatus to the plasma membrane.[8] Cx43 turnover is regulated by proteosomal and lysosomal degradation, and the half-life of Cx43 is less than two hours, suggesting that a rapid synthesis and trafficking system operates in cardiac myocytes.[9]

GJ is modulated by the phosphorylation of Cx43 on Ser and Tyr residues. The intercellular communication through Cx43 is decelerated and accelerated by its phosphorylation on Ser368 by protein kinase C and on Ser364 by protein kinase A (PKA), respectively.[10,11] In addition to Ser phosphorylation, phosphorylated Cx43 on Tyr247 and Tyr265 is repressed from junctional communication.[12] In addition to phosphorylation, GJ formation is regulated by Cx43-binding molecules. Cx43 binds to the junctional adhesion molecule-associating proteins zonula occludens-1 (ZO-1) and β-catenin.[13,14] Dominant-negative ZO-1, which dissociates the endogenous ZO-1 from Cx43, disturbs the localization of

Original received May 10, 2005; resubmission received July 12, 2005; revised resubmission received August 11, 2005; accepted August 16, 2005.

From the Department of Structural Analysis (S.F., Y.N., H.F., N.M.), National Cardiovascular Center Research Institute, Suita, Osaka; the First Department of Internal Medicine (S.S., Y.S.), Nara Medical University, Kashihara, Nara, Japan.

Correspondence to Naoki Mochizuki, Department of Structural Analysis, National Cardiovascular Center Research Institute, 5-7-1 Fujishirodai, Suita, Osaka 565-8565, Japan. E-mail nmochizu@ri.ncvc.go.jp

Circulation Research is available at http://circres.ahajournals.org DOI: 10.1161/01.RES.0000183880.49270.f9

Cx43 at the cell–cell contacts, resulting in the reduced conductance of GJs.[13] Wnt-1 signal prevents β-catenin degradation, thereby increasing β-catenin, which not only drives Cx43 expression but also associates with the Cx43 at the cell–cell contacts, where β-catenin localizes with cadherin.[14]

cAMP-induced Cx43 assembly has been extensively characterized in terms of Cx43 synthesis, delivery to the plasma membrane, and phosphorylation, which is believed to depend exclusively on PKA.[15] However, other downstream molecules of cAMP have not been elucidated in the neoformation of GJs. We and others have demonstrated that exchange protein directly activated by cAMP (Epac)/cAMP-GEF, a guanine nucleotide exchange factor (GEF) for Rap1, is activated by cAMP,[16,17] and that cAMP–Epac-Rap1 signal enhances the barrier function of vascular endothelial cells by stabilizing cadherin-mediated cell adhesion.[18,19] Analogous to this Epac-induced cadherin-based cell adhesion, we hypothesized that Epac may be involved in GJ neoformation as a cAMP-triggered signaling molecule in cardiac myocytes.

In this study, we investigated the molecular mechanism by which GJ neoformation is regulated by cAMP using a PKA-specific activator and an Epac-specific activator. We analyzed the GJ accumulation at cell–cell contacts by immunostaining of Cx43 and the gating function of GJs by dye spreading in neonatal rat cardiomyocytes (NRCMs) stimulated with these activators. We demonstrate that the Cx43 accumulation at cell–cell contacts depends on Epac and that dye spreading depends on PKA. Therefore, PKA and Epac downstream of cAMP cooperatively enhance functional GJ neoformation in cardiac myocytes.

Materials and Methods

Reagents and cAMP Analogs

Dibutyryl-cAMP (dbcAMP) was purchased from Sigma-Aldrich, Epac-specific activator 8-(4-chlorophenylthio)-2′-*O*-methyladenosine-3′,5′-cyclic monophosphate (8CPT) from Calbiochem; and PKA-specific activator N^6-benzoyladenosine-3′,5′-cyclic monophosphate (6Bnz) was from BIOLOG Life Science Institute. Other chemical compounds, antibodies, and adenoviruses are listed in the supplemental information (available online at http://circres.ahajournals.org).

Cell Culture

NRCMs were isolated from Wistar rats (1 to 2 days old; Kiwa Jikken Dobutsu, Japan) on a Percoll gradient as described previously.[20] The details of cardiac myocyte preparation are described in the supplemental information. The NRCMs spread onto the glass-base dishes for 24 hours after isolation were subjected to immunostaining or dye transfer assay after drug treatment for another 12 hours. We observed that the adherens junctions (AJs) were not maturated, although NRCMs contacted each other before the drug treatment, indicating that we used the reassembling NRCMs for the experiments. Experiments using animals were approved by our institutional animal use and care committee. All animal procedures were performed according to the *Guide for the Care and Use of Laboratory Animals* (NIH, revision 1996).

Immunocytochemistry

NRCMs stimulated with cAMP analogs were immunostained as described previously.[21] Briefly, cells cultured on glass-base dish were blocked with PBS containing 4% BSA for 1 hour at room temperature (RT), then stained with anti-Cx43, anti–sarcomeric α-actinin (S-αA), and anti–neural (N)-cadherin at RT. Protein reacting with primary antibodies was visualized with Alexa 488–labeled goat anti-rabbit IgG and Alexa 546–labeled goat anti-mouse IgG. Images were recorded with a confocal microscope (BX50WI; Olympus). For quantitative immunofluorescence analysis, images were also recorded using an epifluorescence microscope (IX-71; Olympus) controlled by MetaMorph version 6.2 software (Molecular Devices). The number of Cx43-positive dots at the cell–cell contacts on the fluorescence images were counted as Cx43 puncta.

Gating Function of GJs Analyzed by Microinjected Dye Transfer

Microinjected dye transfer was performed as described by Doble et al, with minor modifications.[22] The details of dye transfer method are described in the supplemental information.

RT-PCR Analysis

Total RNAs extracted from NRCMs and human cervical carcinoma cell line (HeLa) cells using Trizol (Invitrogen) were reverse-transcribed using SuperScript II and random primers (Invitrogen). The resultant DNAs were PCR-amplified using Epac-specific primers described in the supplemental information.

Western Blot Analysis and N-Cadherin Translocation Assay

NRCMs were lysed in buffer described in the supplemental information. Lysates precleared by centrifugation at 15 000*g* for 10 minutes were subjected to SDS-PAGE and immunoblotting with antibodies as indicated in Figures 3, 4, 5, and 6. Proteins reacting with primary antibodies were visualized by an enhanced chemiluminescence system (Amersham Biosciences) with peroxidase-conjugated and species-matched secondary antibodies and analyzed with an LAS-1000 system (Fuji Film). N-cadherin translocation assay was performed as described previously.[18]

Detection of GTP-Bound Form of Rap1

Rap1 activity was assessed by a modified Bos method as described previously.[23] Briefly, NRCMs starved in DMEM for 3 hours were treated with the stimulants as indicated in Figures 3 and 6 and lysed at 4°C in a pull-down lysis buffer described in the supplemental information. GTP-bound Rap1 was collected on glutathione *S*-transferase fused with Rap1 binding domain of Ral guanine nucleotide dissociation stimulator precoupled to glutathione-Sepharose beads and subjected to SDS-PAGE followed by immunoblotting using anti-Rap1.

Statistical Analysis

The results were expressed as the mean±SD. Student *t* test was used to analyze differences between two groups. Group differences were assessed with one-way ANOVA or two-way ANOVA, followed by post hoc comparisons tested with Scheffe's method. At least 3 fields randomly selected from each culture for analysis of Cx43 staining or at least 4 cells for dye transfer assay from each culture were used to yield a single value for each culture. The number of the cultures for analysis was indicated in the figure legends as n. Significant differences were indicated as P value <0.05 (*).

Results

cAMP Enhances Functional GJ Neoformation in Cultured NRCMs

Because cAMP has been reported previously to enhance GJ formation,[7] we confirmed the dbcAMP–regulated functional GJ neoformation by quantitatively analyzing Cx43 accumulation at the cell–cell contacts by immunostaining and gating function of GJs by microinjected dye transfer assay. dbcAMP enhanced the Cx43 accumulation at the cell–cell contacts (Figure 1A and 1B). To neglect the possibility of cardiac fibroblast contamination in the NRCMs in the following

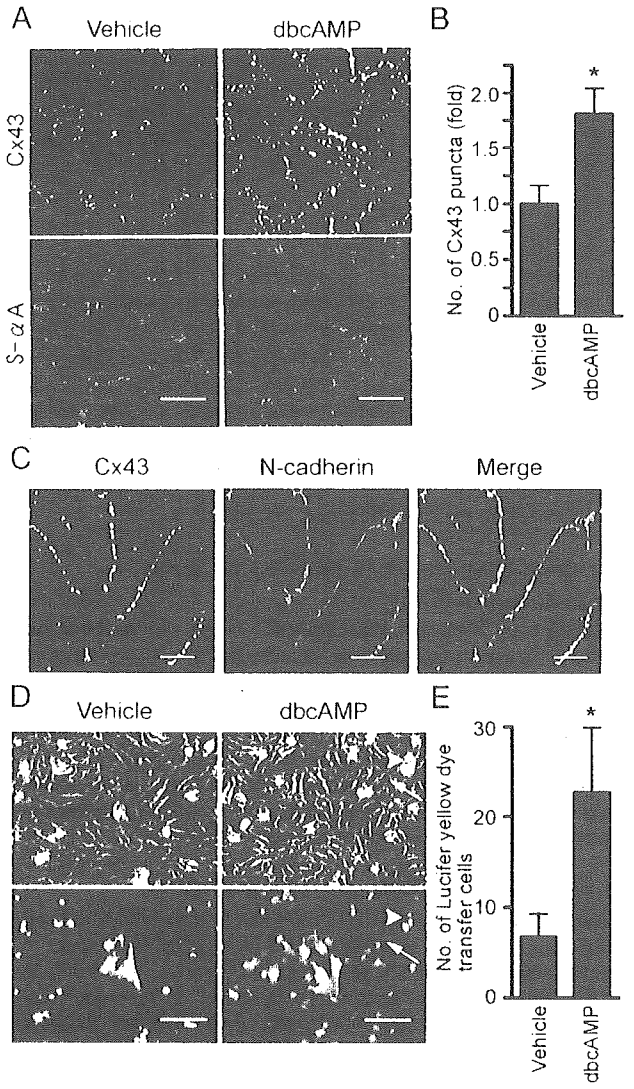

Figure 1. cAMP induces Cx43 accumulation at cell–cell contacts and enhances gap junctional intercellular communication. A, NRCMs cultured 24 hours after cell preparation were stimulated with vehicle or 1 mmol/L dbcAMP for 12 hours. Cells were stained with anti-Cx43 (green) and anti-S-αA (red). Images were obtained through a confocal microscope (BX50WI). Bar=20 μm. B, NRCMs stimulated by dbcAMP were analyzed for Cx43 accumulation by counting the number of puncta at cell–cell contacts. Mean number±SD is expressed as fold increase relative to that observed in the cell treated with vehicle. *$P<0.05$ vs vehicle as analyzed by Student's t test (n=4). Three fields randomly selected from each culture were used for measuring the fold activation between vehicle- and dbcAMP-treated culture by counting Cx43-positive puncta. C, Cells treated with dbcAMP were immunostained with anti-Cx43 (green) and anti–N-cadherin (red). A merged image is shown on the right. Note that puncta for Cx43 are localized to cell–cell contacts as indicated by the N-cadherin immunostaining. Bar=5 μm. D, Microinjected dye transfer assay shows the extent of dye transferring between neighboring cells through GJs. NRCMs stimulated with 1 mmol/L dbcAMP for 12 hours were microinjected with 10% Lucifer yellow. Cells 3 minutes after dye injection were phase contrast imaged (top panels) and fluorescence imaged (bottom panels). Asterisks indicate dye-injected cells. Arrows and arrowheads denote typical dye-transferred cell and cell debris emitting nonspecific fluorescence, respectively. Bar=50 μm. E, Quantitative analysis of D is shown as mean number of dye-positive cells in either vehicle or dbcAMP-treated NRCMs. *$P<0.05$ as analyzed by Student's t test (n=6).

experiments, and to show the confluence of the NRCMs, cells were immunostained for sarcomeric α-actinin (Figure 1A, bottom). The Cx43 puncta in the cells treated with dbcAMP for 12 hours were clearly observed at the cell–cell contacts, where N-cadherin localized (Figure 1C), indicating that dbcAMP induces the accumulation of Cx43 at the cell–cell contacts. We investigated the effect of dbcAMP on gating function of GJs by microinjected dye transfer assays (Figure 1D and 1E). Microinjected dye was more widely transferred to the neighboring cells in dbcAMP-treated NRCMs than vehicle-treated cells (Figure 1D). The quantitative data are shown in Figure 1E. These results are in agreement with previous reports[7,8] and validated the assays we used in this study.

PKA Is Required But Not Sufficient Alone for cAMP-Enhanced GJ Neoformation

Because PKA is involved in the enhancement of GJ formation,[15] we first tested the effect of H89, a specific PKA inhibitor, on cAMP-enhanced accumulation of Cx43. Unexpectedly, H89 did not block the dbcAMP-induced accumulation of Cx43 (Figure 2A and 2B), although H89 did block cAMP-enhanced intercellular communication assessed by microinjected dye transfer assays (Figure 2C).

We next examined the effect of 6Bnz, a specific activator for PKA,[24] on intercellular communication and Cx43 accumulation at cell–cell contacts to directly assess the involvement of PKA in cAMP-enhanced GJ formation. 6Bnz induced Cx43 accumulation slightly but to a much lesser extent than dbcAMP (Figure 2D and 2E). Notably, 6Bnz enhanced dye transfer to a greater extent than vehicle but to a lesser extent than dbcAMP (Figure 2F). These results indicate that PKA signaling is required but not sufficient alone for cAMP-enhanced GJ neoformation and suggest that there is a novel signaling downstream of cAMP in addition to PKA involved in Cx43 accumulation at cell–cell contacts for functional GJ neoformation.

cAMP Activates PKA and Epac-Rap1 Signaling in NRCMs

Epac has been identified as a novel cAMP target and a Rap1-specific GEF. We therefore hypothesized that Epac-Rap1 signaling may be involved in cAMP-enhanced GJ neoformation. RT-PCR analysis revealed the expression of Epac in NRCM but not in HeLa cells used as a negative control (Figure 3A). To test the hypothesis, we first examined whether dbcAMP induces the activation of Rap1 and the phosphorylation of cAMP response element binding protein (CREB) in NRCMs. As shown in Figure 3B, dbcAMP induced Rap1 and CREB activation in NRCMs. Rap1 activation by dbcAMP is dependent on time and concentration (supplemental Figure IA and IB, available online at http://circres.ahajournals.org). H89 inhibited dbcAMP-induced CREB phosphorylation but not dbcAMP-induced Rap1 activation (Figure 3B and 3C), indicating that Rap1 activation does not depend on PKA, whereas CREB phosphorylation depends exclusively on PKA. We next tested whether Rap1 activation and CREB phosphorylation are induced by 8CPT, which has been developed recently as a specific activator for Epac.[25] 8CPT only activated Rap1, not CREB. In striking contrast, 6Bnz induced CREB activation but did not affect

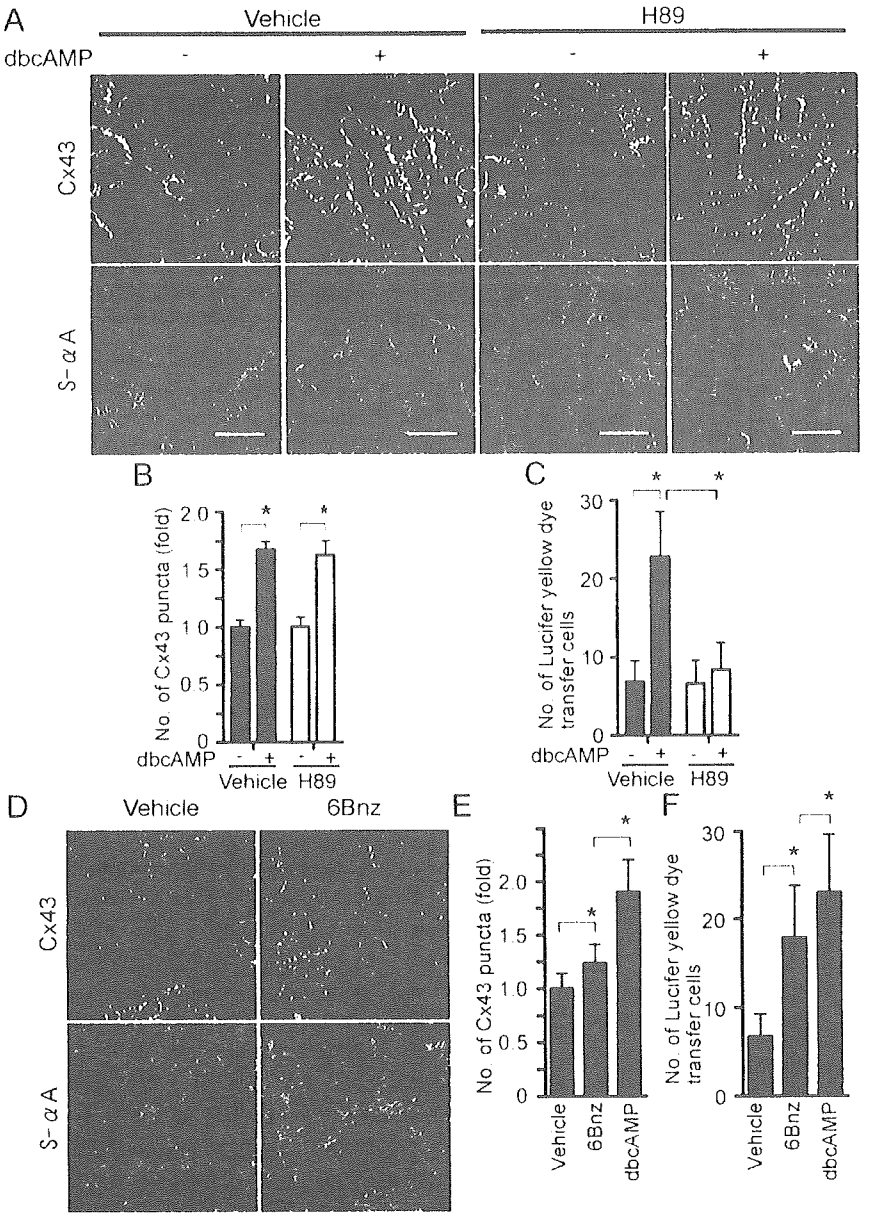

Figure 2. PKA signaling mainly contributes to gating function of GJs. A, NRCMs pretreated with or without 5 μmol/L H89 for 30 minutes were stimulated with or without 1 mmol/L dbcAMP in the presence or absence of 5 μmol/L H89 for 12 hours. After the stimulation, cells were immunostained with anti-Cx43 and anti-S-αA as described in Figure 1A legend. Bar=20 μm. B, Cx43 accumulation in cells treated as in A was quantitatively analyzed. Statistical significance between groups was analyzed by two-way ANOVA with Scheffe's method, indicating that the factor of with/without dbcAMP is significant but not that of vehicle/H89 (*P<0.05; n=6) C, Effect of H89 on dbcAMP-enhanced gap junctional intercellular communication was evaluated by microinjected dye transfer assay as described in Figure 1E legend. Statistical significance between groups was analyzed by two-way ANOVA with Scheffe's method, indicating that both factors, with/without dbcAMP and vehicle/H89, are significant (*P<0.05; n=6). D, NRCMs were stimulated with either vehicle or 1 mmol/L 6Bnz for 12 hours and immunostained with anti-Cx43 and anti-S-αA. Bar=20 μm. E, The effect of 1 mmol/L 6Bnz on Cx43 accumulation at the cell–cell contacts was evaluated similarly to Figure 1B. Statistical significance between groups was analyzed by one-way ANOVA with Scheffe's method (*P<0.05; n=4). F, The effect of 6Bnz on junctional intercellular communication between NRCMs was similarly evaluated by microinjected dye transfer assay to the Figure 1D. Statistical significance was evaluated by one-way ANOVA with Scheffe's method (*P<0.05; n=4).

Rap1 activity (Figure 3D and 3E). Together, these findings demonstrate that cAMP activates Epac-Rap1 and PKA signaling pathways in NRCMs.

Activation of Epac Signaling Leads to Cx43 Accumulation at Cell–Cell Contacts

Because we observed Rap1 activation in response to dbcAMP, we proceeded to investigate the involvement of Epac-Rap1 signaling in cAMP-induced Cx43 accumulation at cell–cell contacts. Like dbcAMP, 8CPT significantly enhanced the accumulation of Cx43 at the cell–cell contacts (Figure 4A and 4B). 8CPT induced Cx43 accumulation at the cell–cell contacts to a similar extent to dbcAMP and to a greater extent than 6Bnz. 6Bnz only slightly increased the number of Cx43 puncta (Figure 4B) compared with vehicle and did not further increase the accumulation of Cx43 at cell–cell contacts caused by 8CPT alone. These results indicate that Epac-mediated signaling is mainly responsible for cAMP-induced Cx43 accumulation at the cell–cell contacts.

We excluded the possibility that increased synthesis of Cx43 on cAMP stimulation resulted in the accumulation of Cx43 at the cell–cell contacts. No discernible increase was observed in the cells stimulated with vehicle, dbcAMP, 8CPT, 6Bnz, and a combination of 8CPT and 6Bnz for 12 hours (Figure 4C and 4D), suggesting that distribution or functional augmentation of GJs is essential for cAMP-induced functional GJ neoformation. In addition, phosphorylation of Cx43 was not affected by dbcAMP, 8CPT, or 6Bnz, nor a combination of 8CPT and 6Bnz (Figure 4C and 4E).

Epac Enhances AJ Formation

Several lines of evidence suggest that AJ formation organized by N-cadherin is a prerequisite for GJ assembly in cardiomyocytes when reassembling and recoupling.[26–28] We used reassembling NRCMs before drug treatment. Recently, we and others revealed that Rap1 is involved in the cell–cell contacts mediated by epithelial (E)-cadherins and vascular

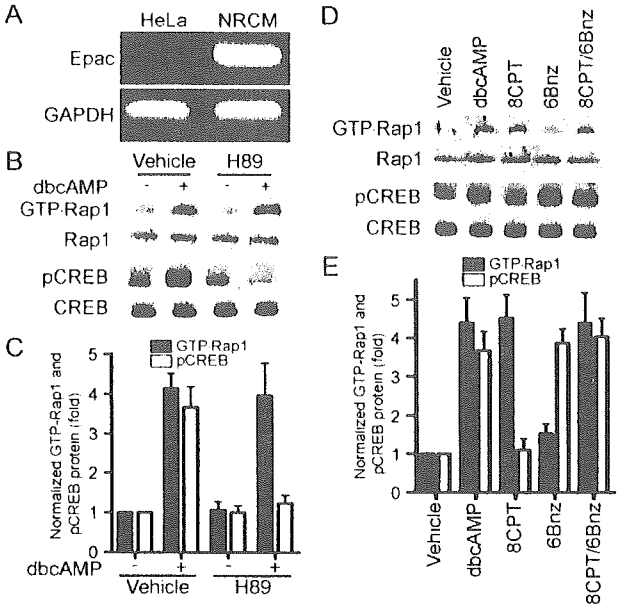

Figure 3. cAMP induces Epac-Rap1 signal as well as PKA signal in NRCMs. A, RT-PCR analysis shows the expression of Epac in NRCMs but not in HeLa cells (used as a negative control). GAPDH was shown as a positive control for RT-PCR. B, Serum-starved NRCMs were stimulated with 1 mmol/L dbcAMP in the absence or presence of H89 for 15 minutes. GTP-bound Rap1 were assessed by pull-down assay. Phosphorylation of CREB was analyzed by Western blot analysis using anti-CREB and anti-phospho-CREB (pCREB). A representative result of 3 independent experiments is shown. C, Data obtained from 4 independent experiments were analyzed quantitatively. Fold activation indicates the ratio of the poststimulation GTP-Rap1 and pCREB intensity of total Rap1 and CREB intensity to the prestimulation GTP-Rap1 and pCREB intensity of total Rap1 and CREB intensity. D, Serum-starved NRCMs were stimulated with either vehicle, 1 mmol/L dbcAMP, 1 mmol/L 8CPT, 1 mmol/L 6Bnz, or 1 mmol/L 8CPT and 1 mmol/L 6Bnz for 15 minutes. GTP-bound Rap1 and phosphorylation of CREB were assessed as described in B. E, Data obtained from 4 independent experiments were analyzed similarly to C.

endothelial-cadherins (VE-cadherins).[18–20] Thus, it is possible that cAMP enhances GJ neoformation by enhancing N-cadherin–mediated AJ formation preceding the GJ formation in NRCMs. To address this possibility, we investigated whether cAMP induces N-cadherin–mediated AJ formation in NRCMs. N-cadherin distribution at cell–cell contacts was enhanced by dbcAMP and 8CPT, whereas 6Bnz neither affected the distribution of N-cadherin nor enhanced the effect of 8CPT (Figure 5A).

To quantitatively analyze the localization of N-cadherin after drug treatment, we performed a biochemical N-cadherin translocation assay. Because N-cadherin is connected to actin cytoskeleton in maturated AJs, cadherin anchored to actin cytoskeleton can be detected in detergent-insoluble fractions of cell lysates. We found an increase in N-cadherin in Triton X-100–insoluble fraction when stimulated by dbcAMP and 8CPT (Figure 5B). However, 6Bnz did not change either basal- or 8CPT-increased levels of N-cadherin in the Triton X-100–insoluble fraction (Figure 5B and 5C). Collectively, these findings indicate that cAMP enhances AJ formation through Epac in NRCMs. We found no difference in N-cadherin expression in NRCMs stimulated with dbcAMP, 8CPT, or 6Bnz, or a combination of 8CPT and 6Bnz by immunoblotting (data not shown).

Rap1 Activation Is Essential for cAMP-Mediated Cx43 Redistribution and AJ Formation

We investigated the role of Rap1 in cAMP-induced Cx43 accumulation and AJ formation in NRCMs. To examine the effect of Rap1 on AJ and GJ formation, we inactivated Rap1 by adenovirus-expressing Rap1GAP1b, which specifically catalyzes the hydrolysis of GTP to GDP on Rap1.[30] Endogenous Rap1 activity was almost completely suppressed by the expression of increasing amount of Rap1GAP1b in NRCMs (Figure 6A). Moreover, overexpression of Rap1GAP1b inhibited cAMP-induced Rap1 activity without affecting cAMP-stimulated CREB phosphorylation (Figure 6B), confirming that Rap1GAP1b specifically blocks Epac-Rap1 pathway but not PKA-mediated signaling.

Inactivation of Rap1 blocked the cAMP-induced accumulation of Cx43 and N-cadherin at the cell–cell contacts (Figure 6C and 6D). dbcAMP-induced translocation of N-cadherin to cytoskeleton-anchored fraction was inhibited by inactivation of Rap1 but not by LacZ overexpression (Figure 6E and 6F). These results suggest that cAMP induces N-cadherin–based AJ assembly through an Epac-Rap1 signaling pathway, which may precede the accumulation of Cx43-based GJs.

PKA and Epac-Rap1 Signaling Cooperatively Enhances GJ Neoformation in NRCMs

Because we found that PKA alone is not sufficient for cAMP-enhanced GJ neoformation and that Epac-Rap1 signaling is involved in cAMP-induced accumulation of Cx43, we assessed the effect of PKA activation and Epac-Rap1 activation on gating function of GJs. 8CPT merely showed the weak enhancement of the intercellular connection, as revealed by microinjected dye transfer assay (Figure 7A). However, 8CPT significantly enhanced 6Bnz-mediated intercellular communication (Figure 7B). The effect of the combination of 8CPT and 6Bnz was comparable to that of dbcAMP. Given that 8CPT induces the Cx43 accumulation at the cell–cell contacts, cAMP potentiates functional GJ neoformation via a PKA-mediated enhanced gating function and Epac-Rap1 signal-mediated accumulation of Cx43 to cell–cell contacts.

Discussion

The function of GJs in the heart depends on the number of GJs between neighboring cells and the gating function of individual GJ at the cell–cell contacts. We investigated how cAMP induces Cx43 accumulation at cell–cell contacts and enhances gating function in NRCMs that were about to develop the mature cell–cell contacts. For the first time, we demonstrated the involvement of Epac-Rap1 signaling downstream of cAMP in GJ neoformation of cardiomyocytes. Although Cx43 accumulated at the cell–cell contacts on cAMP stimulation has been ascribed to PKA,[7] this study demonstrated that Epac-Rap1 signaling activated by cAMP is mainly responsible for the redistribution of Cx43 to cell–cell contacts.

The number of GJs was increased by Epac-Rap1 downstream of cAMP as indicated by the increase in Cx43-positive puncta at cell–cell contacts. However, there was no increase in the amount of Cx43 after cAMP treatment, indicating the importance of the redistribution of Cx43 rather than increase of Cx43 transcription on cAMP. How does Epac signaling induce the accumulation of Cx43 at cell–cell contacts?

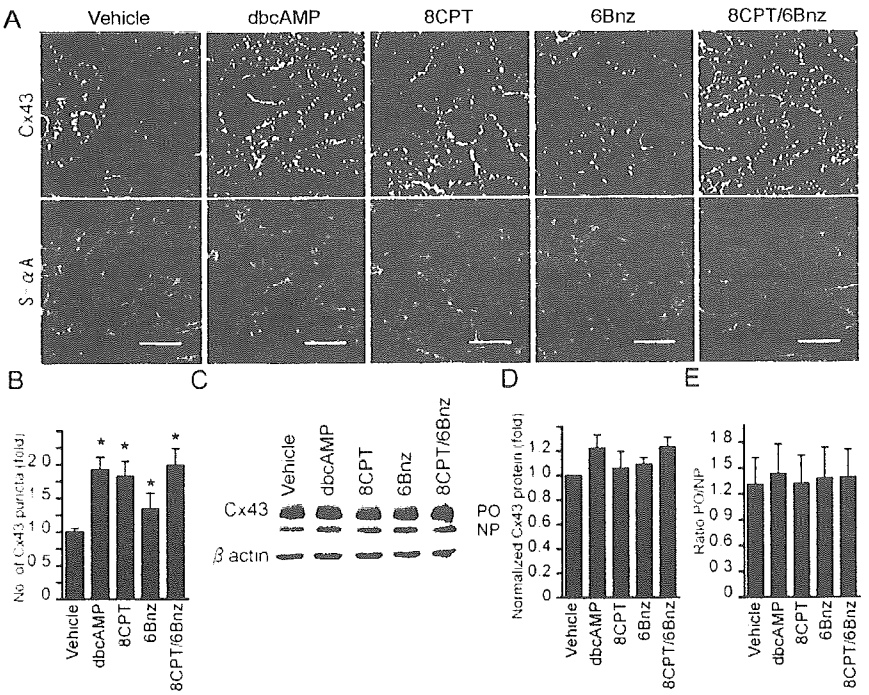

Figure 4. Activation of Epac signaling induces Cx43 accumulation at cell–cell contacts. A, NRCMs stimulated for 12 hours with drugs as indicated at the top were stained with anti-Cx43 and anti-S-αA as described in Figure 1A legend. Bar=20 μm. B, Cx43 accumulation was quantitatively analyzed in Figure 1B. Significant differences between vehicle-treated cells and all drug-treated cells was analyzed by one-way ANOVA with Scheffe's method (*$P<0.05$; n=6). C, NRCMs stimulated as indicated at the top were examined for Cx43 by Western blot analysis. Upper and lower bands correspond to phosphorylated (PO) and nonphosphorylated (NP) Cx43, respectively. D, Total Cx43 (phosphorylated and nonphosphorylated) expression of NRCMs treated for 12 hours with drugs as indicated at the bottom was quantitatively analyzed by three independent Western blot analyses for Cx43. The intensity of the drug-stimulated Cx43 normalized by β-catenin divided by that of vehicle-stimulated Cx43 was expressed as fold activation. E, The ratio is expressed by the intensity of phosphorylated Cx43 (PO) divided by that of nonphosphorylated Cx43 (NP).

Epac-Rap1 activation resulted in enhancement of AJ formation accompanied by GJ formation, as evidenced by increases in N-cadherin and Cx43 at the cell–cell contacts after dbcAMP stimulation (Figure 5). AJ formation constituted by N-cadherin is a prerequisite for GJ neoformation.[28,31] When adult myocytes are cultured, Cx43 is transported and accumulated at the plasma membrane, where N-cadherin accumulates on cell–cell contact.[26] Therefore, GJ formation depends on N-cadherin–based AJ maturation. We have shown previously that the Epac-Rap1 signal enhances the VE-cadherin–based cell–cell contacts in vascular endothelial cells.[18] In this study, we found that Epac activation resulted in the increased accumulation of N-cadherin at the intercellular junction of NRCMs. Thus, N-cadherin accumulation at the cell–cell contacts induced by the Epac-Rap1 signal may account for Cx43 accumulation in NRCMs by analogy to Epac-Rap1–triggered VE-cadherin accumulation in vascular endothelial cells.

The target of activated Rap1 for enhancement of cadherin-based AJ is still unclear. Rac belonging to Rho family GTPase and regulating actin cytoskeleton is suggested to function downstream of Rap1.[32] Therefore, Rac may increase the chances of cell contacts and induce cadherin engagement by extending membrane downstream of Rap1. Maturated N-cadherin on Epac activation, which is detected in the cytoskeleton-anchored fraction, may be accompanied by translocation of Cx43 through cadherin-associating β-catenin

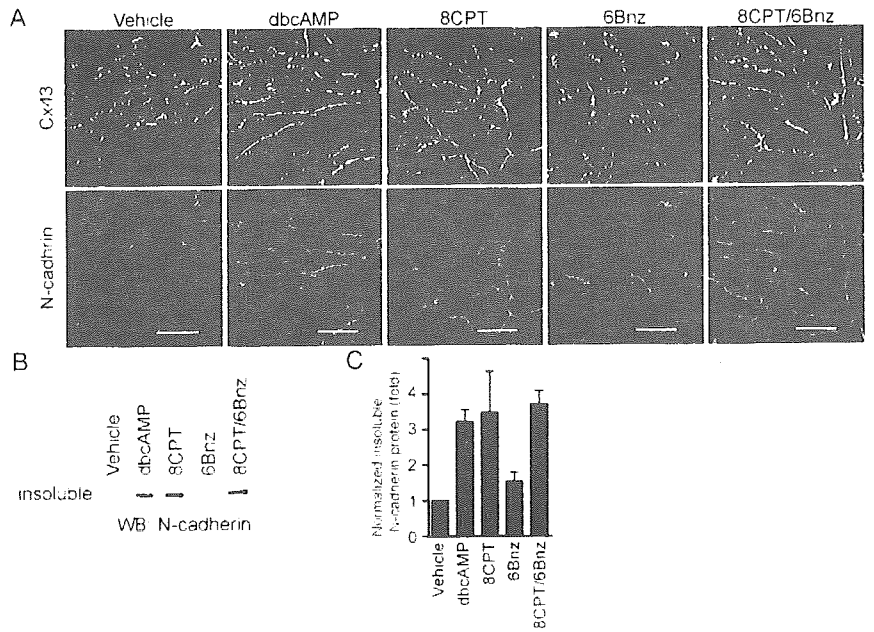

Figure 5. Activation of Epac induces AJ formation. A, NRCMs stimulated for 12 hours with drugs as indicated at the top were immunostained with anti-Cx43 (green) and anti–N-cadherin (red). Bar=20 μm. B, NRCMs stimulated as in A were fractionated with cytoskeleton stabilizing buffer. Triton X-100–insoluble fraction was subjected to SDS-PAGE followed by Western blot analysis (WB) with anti–N-cadherin. A representative result of three independent experiments is shown. C, The data obtained from three independent experiments of B was quantitatively analyzed. The result is indicated as fold increase calculated by dividing the amount of insoluble N-cadherin from the cells treated with the drug by that from the cells treated with vehicle.

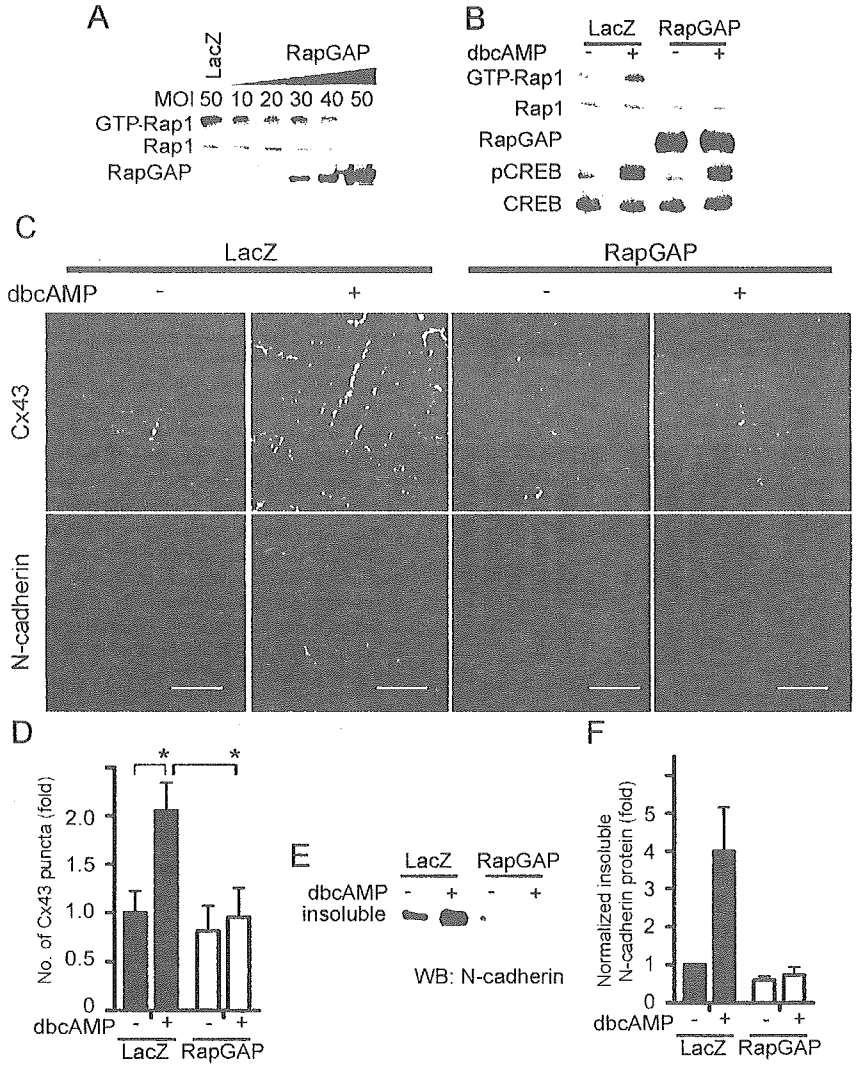

Figure 6. Rap1 activation is required for cAMP-induced Cx43 accumulation at the cell–cell contacts and AJ formation. A, Rap1 inactivation by Rap1GAP1b was verified by detecting GTP-Rap1 in NRCMs infected with different multiplicity of infection (MOI) of adenovirus-expressing Rap1GAP1b (Ad-RapGAP). An adenovirus-expressing LacZ (Ad-LacZ) at 50 MOI was used as a control. GTP-Rap1 was detected by pull-down assay. Rap1 and Rap1GAP1b (RapGAP) expression was examined by Western blot analysis using antibodies as indicated at the left. B, NRCMs infected with either Ad-LacZ or Ad-RapGAP at an MOI of 50 for 24 hours were stimulated with vehicle (−) or 1 mmol/L dbcAMP (+) for 15 minutes and analyzed for Rap1 and CREB activation. C, Localization of N-cadherin and Cx43 was examined similarly to Figure 5A in NRCMs infected with Ad-LacZ or Ad-RapGAP after stimulated with vehicle or 1 mmol/L dbcAMP for 12 hours. Bar = 20 μm. D, The effect of inactivation of Rap1 on dbcAMP-induced accumulation of Cx43 was analyzed by two-way ANOVA with Scheffe's method, indicating that both factors, with/without dbcAMP and LacZ/RapGAP, are significant ($^*P < 0.05$; n = 6). E, Translocation of N-cadherin was examined in NRCMs infected with Ad-LacZ or Ad-RapGAP after stimulation of dbcAMP. A representative of three independent results is shown. F, The three independent results from D were analyzed similarly to Figure 5C.

because Cx43 is capable of binding to β-catenin.[11] Because ZO-1 is recruited to AJs by binding to α-catenin and is also capable of binding to Cx43,[33] ZO-1 may participate in the accumulation of Cx43 during maturation of AJs.

Another factor affecting functional GJ neoformation in addition to the number of GJs is the gating function of individual GJs. PKA activation facilitates intercellular communication without accumulation of Cx43 at cell–cell contacts, concurring with previous reports underpinning that PKA and cAMP increases single channel conductance of the GJ,[9] although the characteristics of single GJ channel conductance evoked by PKA activation still remains elusive.[15] We found a marked increase in dye transfer on PKA activation with a slightly increased accumulation of Cx43 at the cell–cell contacts (Figures 4 and 7). These results indicate that PKA mainly contributes to the functional neoformation of GJs by enhancing gating function of GJs. Phosphorylation of Cx43 on Ser residues is required for intercellular communication of GJs.[16] Because we found no significant increase in either total Cx43 or phosphorylated Cx43, PKA may indirectly modulate GJ conductance in addition to direct phosphorylation of Cx43 or may phosphorylate a critical Ser/Thr that was indistinguishable in the phosphorylated Cx43 band in our immunoblot for Cx43 (Figure 4C).

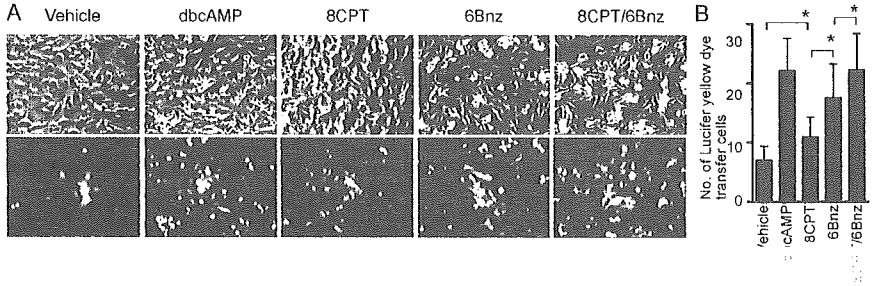

Figure 7. PKA signal and Epac-Rap1 signal cooperatively enhance intercellular communication through GJs. A, Intercellular communication was assessed by microinjected dye transfer assay using NRCMs stimulated with drugs as indicated at the top. B, Dye spread was quantitatively analyzed similarly to Figure 2F. Statistical significance between groups was evaluated by one-way ANOVA with Scheffe's method ($^*P < 0.05$, n = 6).